DD

Fermi National Accelerator Laboratory

CERN LIBRARIES, GENEVA
P00022862

FERMILAB-FN-608

SW 9418

# Apparatus for Magnetic Moment Measurement Using Channeling in Bent Crystals

V.V. Baublis, V.V. Ivanov, V.G. Ivochkin, A.V. Khanzadeev, V.V. Kuryatkov, E.G. Lapin, N.M. Miftakhov, V.F. Morozov, S.R. Novikov, T.I. Prokofieva, V.M. Samsonov and G.P. Solodov

*Petersburg Nuclear Physics Institute*
*Gatchina, Russia*

B.D. Dvornikov, A.A. Kochenova, Y.E. Kolesov and B.B. Loginov

*SRI Electron*
*St. Petersburg, Russia*

R.A. Carrigan, Jr. and D. Chen

*Fermi National Accelerator Laboratory*
*P.O. Box 500, Batavia, Illinois 60510*

January 1994

Operated by Universities Research Association Inc. under Contract No. DE-AC02-76CHO3000 with the United States Department of Energy

# Disclaimer

*This report was prepared as an account of work sponsored by an agency of the United States Government. Neither the United States Government nor any agency thereof, nor any of their employees, makes any warranty, express or implied, or assumes any legal liability or responsibility for the accuracy, completeness, or usefulness of any information, apparatus, product, or process disclosed, or represents that its use would not infringe privately owned rights. Reference herein to any specific commercial product, process, or service by trade name, trademark, manufacturer, or otherwise, does not necessarily constitute or imply its endorsement, recommendation, or favoring by the United States Government or any agency thereof. The views and opinions of authors expressed herein do not necessarily state or reflect those of the United States Government or any agency thereof.*

Fermilab-FN608

# APPARATUS FOR MAGNETIC MOMENT MEASUREMENT USING CHANNELING IN BENT CRYSTALS

V. V. Baublis, V. V. Ivanov, V. G. Ivochkin, A. V. Khanzadeev, V. V. Kuryatkov, E. G. Lapin, N. M. Miftakhov, V. F. Morozov, S. R. Novikov+, T. I. Prokofieva, V. M. Samsonov, G. P. Solodov

Petersburg Nuclear Physics Institute, Gatchina, Russia

B. D. Dvornikov, A. A. Kochenova, Y. E. Kolesov, B. B. Loginov

SRI "Electron" (St. Petersburg, Russia)

R. A. Carrigan Jr., D. Chen

Fermi National Accelerator Laboratory, Batavia, IL 60510

## ABSTRACT

A recent experiment has demonstrated spin precession using a bent channeling crystal for the first time. The experiment studied the precession of 375 GeV/c $\Sigma^+$ hyperons in silicon crystals bent through 1.6 mrad. In the course of carrying out the experiment defect dechanneling was studied and dechanneling from dislocation slip planes was observed for the first time. System spatial and angular resolution was good enough to examine crystal distortions and observe their impacts. New insights were gained concerning techniques for implanting detectors on channeling crystals. Sophisticated pre-alignment schemes were used to set crystal bending angles and orientations using x-ray diffraction techniques. The experiment was one of the first channeling experiments to employ multiple crystals. The ramifications of this experiment for trans-TeV channeling are explored.

## 1. INTRODUCTION

In the last several years possible applications of particle channeling in bent crystals have attracted attention in different fields of high energy physics. These have included the possibility of forming secondary beams[1], beam extraction from accelerators[2], beam focusing elements[3], and a measuring instrument to determine beam emitance[4]. Now a recent experiment[5] has demonstrated the possibility of applying bent crystal channeling to the measurement of the magnetic moments of short-lived particles.

Bent crystal channeling could potentially play a significant role for beam extraction from multi-TeV accelerators such as LHC[6] for fixed target experiments and for the measurements of magnetic moments of short-lived particles such as charm baryons. However these applications require new understanding of accelerator extraction[7], as well as a greater depth of understanding of the technical aspects of channeling including new challenges for crystal quality, goniometers, and experimental apparatus.

During the preparation and execution of the experiment to observe the spin precession of the $\Sigma^+$ hyperon measurement at 375 GeV many systematic investigations of the technical elements related to channeling were carried out. These included development of techniques for selecting crystals and testing crystal quality, processing and precisely orienting crystals, and implanting diodes used as particle detectors on the oriented crystals. New methods were devised for supporting bending crystals. In addition, a precision goniometer system was designed, built, and operated.

As the channeling precession experiment is unique both from the standpoint of precision and the approach, it is useful to review the experience gained in its preparation and performance. It is also interesting to examine that experience in light of the requirements for future channeling applications at trans-TeV accelerators like the LHC. A condensed version of this article will appear in Nuclear Instruments and Methods[8]

## 2. THE $\Sigma^+$ EXPERIMENT

Shortly after Tsyganov[9] first noted that channeled particles moving in a curved crystal should be deflected, Baryshevskii[10] and Pondrom[11] pointed out that the magnetic moment of a channeled particle should precess in a bent crystal. The detailed theory has been treated by Lyuboshits[12] and Kim[13]. In a curved crystal the net electrostatic field of the atomic planes deflecting the particle transforms into a magnetic field in the particle's rest frame. The spin precession angle $\phi$ is:

$$\phi = \gamma\omega(g-2)/2 \qquad (\text{for } \gamma \gg 1) \qquad (1)$$

where $\gamma$ is the Lorentz factor, g is the g factor, and $\omega$ is the deflection angle of the channeled particle. Since the values of $\phi$, $\omega$, and $\gamma$ are known, g can be determined. The magnetic moment is:

$$\mu = (gq/2mc)\cdot S \qquad (2)$$

where q, m, and S are respectively the charge, mass, and the spin of the particle. For a 375 GeV/c $\Sigma^+$ hyperon and a deflection angle of $\omega$ = 1.65 mrad, $\phi$ should be 1 rad. For a 45 mm crystal the equivalent laboratory field is 45 Tesla. Channeling could be preserved for bends up to twenty times as large leading to equivalent fields of order 1000 T.

In the E761 experiment we studied the rotation of the polarization vector of channeled $\Sigma^+$ hyperons in bent crystals using a general-purpose spectrometer system (Fermilab E761) in the Fermilab P-Center beam. The spectrometer system was employed for a variety of other investigations including measurements of the polarization[14] of the $\Sigma^+$, the asymmetry parameter[15] for polarized $\Sigma^+ \to p\gamma$, and a conventional $\Sigma^+$ magnetic moment measurement[16]

The top portion of Fig. 1 shows a schematic of the experiment. A vertically polarized $\Sigma^+$ beam[17] was produced by deflecting the 800 GeV/c proton beam on to the production target (T) horizontally at ±3.7 mrad. The beam polarization of 12±1% was obtained by measuring the $\Sigma^+ \to \pi^\circ p$ decay asymmetry in the baryon spectrometer for non-channeled sigmas. Sequential runs were taken with alternating polarizations. The hyperon beam at the crystals was 18 mm high (FWHM) with a vertical angular extent of 1.4 mrad. The beam 10 m from the production target consisted of about 1% $\Sigma^+$ hyperons mixed with protons and relatively long-lived particles such as pions. The spectrometer system operated with a beam flux of 100 KHz.

The hyperon spectrometer[18] consisted of a system of silicon planes and a magnet. This was followed by a 14 m decay region and a baryon spectrometer of magnets and proportional planes. The resolution in the hyperon spectrometer ($\sigma$) at the crystals was 7 µrad for the vertical angle and 15 µm in space, set mainly by the 50 µm spacing in the silicon strip detectors.

The channeling apparatus is shown in the lower part of Fig. 1. An array of silicon crystals with (111) planes close to the horizontal was positioned after the hyperon spectrometer near the upstream end of the decay region. A remotely-controlled goniometer capable of 1.8 μrad steps in $\psi_y$ (the projected angle of the crystal) was used to orient the array. The bends in the upper crystals deflected down -1.649±0.030 mrad while the lower crystals deflected up by the same amount. Deflection angles were measured using long-lived, channeled particles. Crystal curvature around the horizontal axis (the x axis) perpendicular to the beam direction (z) produced an equivalent magnetic field $B_x$ which precessed the hyperon spin in the (y,z) plane. Eight diode detectors each 2.5 mm long in the beam direction were implanted along the 45 mm long, 400 μm thick crystals to measure energy loss. The crystals were aligned by varying $\psi_y$ to find the anomalously low energy loss characteristic of channeled particles and the large angular deflections due to channeling in the bent crystals.

The fraction of the beam area subtended by the active area of one crystal was 0.4%. The fraction of the beam on a crystal that channeled depended on the phase space matching to the channeling critical angle[19] and dechanneling effects. The critical angle is about 10 μrad for a 375 GeV/c $\Sigma^+$ hyperon moving between the wide (111) planes in silicon. The vertical angular divergence of the portion of the beam incident on a crystal was 72 μrad FWHM.

The observed transmission of channeled particles through the crystal was 50% of the expected transmission[20]. However the error on the estimate amounts to a factor of two. In a future experiment straight-forward improvements could improve the spatial acceptance by a factor of twenty-five.

A special trigger significantly enhanced the number of channeled particles recorded on tape. The trigger required a signal greater than 1/20th of the most probable random energy loss from an upstream crystal diode in coincidence with a hyperon spectrometer count and in anti-coincidence with a downstream veto counter (DF). The height of DF in the beam after the baryon spectrometer was adjusted so that the channeled $\Sigma^+$ decay proton would not pass through it but most beam-associated particles would. A remotely-controlled and precisely-aligned anti counter (A) upstream of the goniometer with holes over the crystals reduced the trigger rate and thereby increased the data collection rate.

## 3. SELECTING AND TESTING CHANNELING CRYSTALS.

Channeling can be quite sensitive to various defects in crystal structure. These include macroscopic defects (dislocations, twins, and stacking faults) as well as micro-defects (agglomerations of point defects) and also swirl defects[21]. As a result, in preparing a channeling experiment it is important to devote special attention to the investigation of defects in the starting material. Typically this starting material is a single crystal of silicon.

With increasing particle energy the requirements for perfect crystal lattice structure becomes more crucial. The existence of any defects causes distortion of some region of the lattice and, correspondingly, dechanneling in the region around the defect. The size of this region effectively depends on the incoming particle energy. Fig. 2 from a discussion by Samsonov[22], illustrates this process for dislocations. Dechanneling of particles on dislocations results from the fact that dislocations cause local deformation of the crystal lattice (bending, in particular). When particles moving in the channel get into the deformed region of the crystal they are subjected to the effect of a centrifugal force and are scattered at large angles at the point of interaction with the center of the dislocation. One of the characteristics of such a process is the size of the so-called "dechanneling cylinder" around the dislocation. That is the region of the deformed lattice where the channeling particle cannot stay in the channel and leaves it, that is, dechannels (Fig. 2). The radius of the dechanneling cylinder in the case of planar channeling is different for different types of dislocations--edge dislocations, screw dislocations, dislocation loops, etc. Assuming that all types of dislocations are present in the crystal and their locations are averaged in all directions relative to the trajectory of the particle, the radius of the generalized dechanneling cylinder will be[23]:

$$r_0 = \lambda/2 = 1/2(lE_p/k_2 z_1 z_2 e^2 N_p)^{1/2} \qquad (3)$$

Here $E_p$ is the energy of the particle, $ez_1$ is the charge of the incoming particle, $z_2$ is the atomic number of the element forming the lattice, $l = d_{(111)} = 3.14$ Angstroms is the magnitude of the Burgers vector for the dislocation, $N_p = 0.161/A_2$ is the atomic density in the plane and $k_2 = 8.6$ is the constant coefficient (for edge dislocations $k_2 = 4.5$, for screw dislocations $k_2 = 12.5$). From this equation one can easily estimate that for $E_p = 375$ GeV, the energy of the Fermilab E761 channeling spin-precession experiment, the size of the forbidden zone is $2r = 6.5$ microns. For $E_p = 20$ TeV it will be $2r = 47$ microns. For this reason the selection of the starting silicon for crystal preparation is very significant for high energy channeling experiments.

For the E761 experiment, single crystal n-type phosphorus-doped silicon with a resistivity in the range 5-20 KΩ•cm was used. This material was produced at Zaporozhie Metallurgical Company (Ukraine) by the float-zone melting technique. The starting ingot was grown with a <111> axis along the axis of the ingot. It was 62 mm in diameter, 100 mm in length, and weighed 710 g. Along a radius of the ingot the resistivity variation was less than 35% while along the axis the variation was in the range 5-20 KΩ•cm (Fig. 3). According to the manufacturer, the minority carrier lifetime ranged from 2200 to 2400 μs. The manufacturer also specified that the oxygen and carbon concentrations were less than $10^{+16}$ $cm^{-3}$. High resistivity silicon was necessary because of the requirement that the crystal also serve as a semiconductor with a 400 μm depletion depth[1].

The silicon ingot was cut into 40 round wafers with their large faces parallel to a (111) plane. Each wafer was 450 microns thick and 62 mm in diameter. These wafers were then investigated for defects. Two methods were used:

- a traditional chemical selective-etching technique to reveal dislocations and clusters;

- a new Si-H film decoration technique (designated FDT below) to observe dislocations, clusters, impurities, and structure defects.

The chemical selective etching method showed that none of the starting wafers had dislocations appearing at their surfaces.

The application of this new FDT has already shown its effectiveness for the analysis of silicon crystals used in photo-electrical device fabrication[24]. The method consists of forming both a macro and micro pattern that is obtained as a result of the color contrast made by the product of the chemical reaction between Si and the decorating solution. The rate of such a reaction is rather sensitive to the structure homogeneity of the silicon surface and has different values in regions that have defects or are free of defects. Variations over different wafer regions with different inhomogeneities can be easily evaluated by the color differences of the reaction products, which arise from the interference of the light reflected from the internal and external boundary of the silicon-film system.

The film substance is more chemically active than the silicon due to Si-H bonds. It can be easily removed from the surface

---

[1] Note that the need for high resistivity was not connected with the requirement for an absence of crystal structure defects.

without any material destruction except for a thin silicon layer of 600-800 Angstroms involved in the film formation.

The FDT method used here has an advantage over the widely used selective etching technique due to its high sensitivity. In addition, it is a non-destructive technique. Wafers examined in such a way can be used later for production of devices. The FDT method has been used for the development of the technology and production of microstrip detectors[25]. At present we are continuing the investigation of other possible applications of this technique.

The film decorating results for four starting silicon wafers are shown in Fig. 4. Concentric rings are visible in several of the wafers. These are due to inhomogeneous distributions of point defects and clusters during the growth of the crystal. The visibility of the small inhomogeneities illustrates the potential of this technique to select samples free of problems. For high resistivity silicon wafers we have succeeded in revealing mechanical surface defects such as scratches, marks, and micro-cracks with the same technology as with low resistivity silicon. However, sometimes we are not able to reveal surface inhomogeneities of high resistivity silicon in detail due to an impurity content that is lower (by several orders of magnitude) in comparison to low resistivity wafers. The impurity inhomogeneity values shown in Fig. 4 indicate the difference in the distribution of doping impurities, which is in agreement with SHF (Super High Frequency method)-profiling measurements of resistivity ($\rho$)and minority carrier lifetime ($\tau$) (Fig. 5). Thus, for the most homogeneous wafer (#3) the $\rho$ variation is 16% and the $\tau$ variation is 8% while for the wafer with the swirl inhomogeneities (#4) the variation of $\rho$ and $\tau$ is equal to 69% and 40%.

The FDT technique confirmed the absence of dislocations in the starting silicon wafers but revealed significant concentrations of point defects and clusters especially for wafers from the higher resistivity (7-20 KΩ•cm) portions of the ingot.

The E761 channeling crystals consisted of 25 mm * 45 mm plates with eight implanted detector diodes spaced along the 45 mm length. Each detector was 13 mm wide and 2.5 mm along the beam direction. Wafers were selected which were homogeneous enough in resistivity so that they were suitable for the preparation of diode structures of the needed dimensions. Twenty samples were selected with resistivity in the 5-6 KΩ•cm range.

On the basis of these investigations we believe future experiments on beam extraction from the SSC and LHC accelerators could choose starting material silicon with a resistivity of 1-2 KΩ•cm. It is possible to have silicon of this resistivity

without any dislocations and, apparently, with minimal inhomogeneity in the distribution of point defects and clusters. This material is less expensive than silicon in the 10 KΩ·cm range.

## 4. PROCESSING, ORIENTING, AND CHARACTERIZING THE CRYSTALS.

The nature of the E761 experiment and apparatus required that the (111) plane be closely aligned with the major face of the crystal. With that in mind, careful attention was paid to aligning the crystal planes with the body of the crystals.

Before cutting the crystals an X-ray spectrometer was used to determine the orientation of the ingot (111) plane which was almost perpendicular to the <111> axis of the ingot growth. The direction of one of the (110) planes perpendicular to the (111) plane was also determined. The accuracy of the plane direction measurement was $(1\text{-}2)*10^{-4}$ radians. The determination was limited by the precision of the spectrometer.

Next a small slice was made along the whole ingot along the (110) plane. The aim of this procedure was to have an absolutely fixed orientation of the crystal structure relative to the surfaces of all the slabs. After that orientation the ingot was sliced along the (111) plane. The alignment was periodically tested and the cutting procedure corrected.

The angle $\theta$ (see Fig. 6a) between the (111)-plane and the surface of the processed plates was also measured with an X-ray spectrometer. These measurements showed that for the main group of wafers (30 plates) the divergence in the angle $\theta$ was $\langle\theta\rangle < 3*10^{-4}$ radians (see Fig. 6a). For the rest of the wafers $\theta$ ranged from $5*10^{-4}$ to $10^{-3}$ radians.

The plates were polished to a thickness of 400±20 microns. Variations of thickness were less than ±1 micron (see Fig. 6b for a schematic picture). This set an upper limit on the non-parallelism of the surfaces of the plates and for determining the parallelism of the plates in the multiple plate bending system of the goniometer. The wafer surface roughness depended on polishing quality and was approximately equal to 0.05-0.1 µm (Fig. 6c). Note that practically the wafer processing didn't change the angle $\theta$.

The accuracy of the crystallographic plane orientation and nearly parallel surfaces were important for this experiment and is also important for many other channeling experiments. There are a variety of edge effects. For example, if $\theta=3*10^{-4}$ radians for the E761 crystal, planes leak out the sides of the plate for a 27 µm band. For the 400 µm thick E761 crystals this results in a non-functioning portion of 7%. As a result of this non-functioning region, feeding-in and loss of particles from the channels will occur along almost the entire length of the crystal. This will imitate the real processes of volume capture (feeding-in) and dechanneling. In addition, if the crystal incorporates implanted semiconductor detectors and the detectors are not fully depleted, some beam particles passing through the inefficient region due to

the incomplete depletion will have "small" energy losses and will imitate the low energy loss behavior of channeled particles.

The accuracies mentioned for the parameters discussed above satisfied the requirements of E761 but would not satisfy the requirements for SSC and LHC beam extraction and future experiments at higher energies. It is possible to improve the accuracy and achieve a smaller value for the angle $\theta$ and better surface parallelism with modern polishing techniques but it will be necessary to work with more precise measuring systems. For instance, instead of the usual x-ray diffractometer it will be necessary to use a precise two-crystal diffraction device (Fig. 7) in which the first crystal serves as a monochromator and the second is the crystal under investigation. In addition, in this device an optical auto-collimator would be useful to check the position of the crystal surface. With this approach it should be possible to achieve orientation accuracies such that $\theta$ would be less than $\pm 5$ $\mu$rad.

The next stage in the E761 alignment process was to orient other faces of the crystal inside the (111) plane. It is important to not have an accidental alignment of the beam direction (taking into account the beam angular divergence and crystal bending angle) and the directions of other crystallographic planes and axes. This is to rule out the possibility of channeled particles being redistributed from channeling in the (111) plane to channels of other planes and to also exclude the possibility of channeled particles being captured (edge capture as well as volume capture) and channeled by other planes or axes simultaneously with the (111)-plane.

To illustrate this situation, Fig. 8 presents a partial map of the stereographic projection of the intersections of different low index crystallographic axes[26] (corresponding to the intersections of the crystallographic planes perpendicular to these axes) on the (111) plane and inside of a 15 degree limit relative to the (111) plane.

As a result of these facts the orientation of the plates was chosen as shown in Fig. 9. The short edge was cut in a direction rotated 7 degrees to the <110> axis. A fragment of the atomic lattice in the (111) plane relative to the edges of the plate is also shown in this figure.

Because we planned to implant semiconductor detectors on the surfaces of the plates, using the small slice made earlier along the whole ingot in the (111)-plane helped us to orient the plate in the proper way. In the photo-lithography process for making the detectors it was easy to orient the topology of the detectors and plate edges at 7 degrees to this direction and cut plates with the proper orientation from the wafers.

After implanting the detectors and cutting the plates we measured the reverse currents of the diodes and selected ten samples. These samples had the following parameters for the crystallographic plane orientation: $\theta < 5*10^{-4}$ radians, $\eta < 5*10^{-4}$ radians, and $\phi = 7\pm0.5$ degrees. These are shown in Fig. 10.

After all the technical steps of cutting and orienting the crystals and implanting the detectors the next step was the analysis of the silicon material quality using the film decoration technique. At that point evidence for many new macro-defects appeared on the edges of the plates.

Fig. 11 shows the film grown on the surface of one of the crystals after chemical etching of a 30 µm thick layer. As seen in Fig. 11, the films reveal such structure defects as slip lines.

The slip lines[27] are connected with the existence of edge dislocations and their slip at the (111) planes in the <110> directions. The planes and the slip directions compose the slip system. There are four (111) planes and three <110> directions in the silicon lattice. The slip of the dislocations results in the formation of steps on the crystal surface. These steps are exposed on the film as the slip lines. These lines are spaced 60° apart and aligned with the <110> directions. These lines are in good agreement with the slip line directions revealed on the film and the orientation of the crystal cuts established with the x-ray alignment (see Fig. 11).

There can be several reasons for the appearance of the slip. To check the influence of plastic deformation of the crystal in the bending device we used the Si-H film technique to select two eight-pad detectors without slip lines. These were placed in a bending device for several months. No dislocations appeared after bending for two months.

Note that there are slip lines around the edges of the crystals (see Fig. 11). This is probably due to the fact that the edges of the unprocessed wafers serve as a source of slip lines. Mechanical disturbances connected with the preparation of the wafers can serve as sources of slip dislocations under high temperature conditions. We have repeatedly observed such edge slip lines with Si-H films.

The presence of these defects on the edges of plates was probably caused by a technique often used in semiconductor manufacture. In this technique a line is scribed on the silicon and the plate is broken along the line. At this stage it is probably important to use special cutting equipment and then to polish the edges of the plates.

In spite of careful selection of the starting material and strict attention to preparing and processing the plates there is

still a possibility of missing internal defects which have not appeared at the plate surface. This happened for one of the seven crystals prepared for the E761 experiment. It was only during the course of the experiment that we discovered significant dechanneling at the downstream end of this crystal. After completing E761 this plate was analyzed by microscopic observation of the surface after a selective chemical etch to remove a 100 μm thick surface layer. Fig. 12 is a photograph of the plate decorated with the Si-H film. In the central part of detectors 7 and 8 a cluster of different macro-defects and inhomogeneities from impurities was visible. Defect studies using the two-crystal diffraction spectrometer at PNPI confirmed the crystal structure distortion in that part of the crystal. This plate was used as the analyzer in the two-crystal spectrometer (Fig. 13). First this Laue-Laue type spectrometer was tuned for diffraction from the (404) plane. The diffraction line width was then measured at different points along the crystal as the plate was shifted parallel to the first crystal. The dashed lines in Fig. 14 show the exposed regions of the crystal. The solid lines show the cross-section of the x-ray beam on the surface of the plate.

Fig. 15a shows the two-crystal lines for two positions of the x-ray beam on the crystal surface (L=0; L=42.5 mm). The width (FWHM) of the two-crystal line measurements for all measured x-ray positions on the crystal surface are presented in Fig. 15b. It can be clearly seen that the diffraction peak in the region of L=30-45 mm (pads 6-8) is about four times wider than in the upstream portion of the crystal.

## 5. IMPLANTING DETECTORS ON THE CRYSTALS.

After a wafer was oriented and its surface was prepared, semiconductor detectors were implanted on the wafer surface. The detectors were prepared at the research institute and production facility "Electron" (St. Petersburg, Russia) with the technique that is normally employed for production of electronic components utilizing low resistivity silicon technology.

A schematic layout of the detector array is shown in Fig. 16. The array consisted of eight sensitive elements, each with an area of 2.5 x 13 $mm^2$ and with a 3 mm separation between each of the pads. The array was fabricated on a 45 x 25 $mm^2$ slice of silicon.

The layout of the sensitive elements and the signal outputs from them was chosen to eliminate any contact with the bending device used in the E761 experiment.

The cross-section of the detectors is shown in Fig. 17. The p-n junction was produced by boron diffusion from a boron-doped, poly-silicon layer $Si^*(B)$. The $n^+$-layer was made by phosphorus implantation on the obverse side with an implantation energy of 110 KeV and a fluence of $3.0*10^{15}$ particles/$cm^2$. An aluminum layer with a thickness of about 1 μm was evaporated in vacuum on both sides for the contacts.

The electronic response of these detectors was unexpected. The electronic behavior of the silicon was significantly changed in the process of implanting the detectors.

Fig. 18 shows typical volt-ampere (VA) and volt-farad (VF) characteristics for one of the diodes. While the resistivity of the starting material was in the 5-6 KΩ·cm range, the VF characteristic analysis indicated that the resistivity of the materials after processing was lowered to the 0.5-1.0 KΩ·cm level. This lower resistivity resulted in a smaller depletion depth of 140 to 200 μm for an applied 150 V reverse bias.

The low resistivity and the resulting incomplete depletion was a problem in carrying out the E761 experiment. It resulted in a decrease of the useful crystal thickness by a factor 2-3. The signals from particles passing through the layer that was not depleted had anomalously small amplitudes due to incomplete charge collection. This distorted the amplitude spectra of the channeled particles that passed through that region of the crystal. Since the E761 apparatus had a precise tracking system based on microstrip detectors, it was possible to reject these events from that portion of the crystal. The two dimensional plots in Fig. 19 illustrate the distribution of the amplitudes from one of the detectors for different depths (Y-direction) in the crystal.

With a view toward future experiments we have investigated the circumstances that caused this effect and searched for a way to improve the technical process so that it could be used for high resistivity material. After the experiment was completed an analysis was carried out to determine the cause of the resisti-vity decrease during the production process. New sets of Shottky barrier detectors were implanted on new silicon wafers from the same ingot used for the experiment. As they were produced the material resistivity was monitored after each stage of the production process using deep level transient spectroscopy (DLTS). This method was developed by Lang[28] in 1974. It makes it possible to determine the main parameters of deep energy levels of electrically-active centers at concentrations of $\geq 2 \cdot 10^{-13}$ atomic percents.

The measurements were made using an automatic relaxation DLTS spectrometer developed at the Petersburg Nuclear Physics Institute (PNPI)[29]. With this spectrometer it is possible to study the relaxation of diode capacity produced by deep levels with time constants from $10^{-4}$ to $10^{-1}$ s. This can be done over a temperature range of 77 to 300 °K. In order to do this, the Shottky Si-Au barriers were made at room temperature to avoid introducing any defects. DLTS and resistivity measurements were made after the technical operations connected with the high temperature treatment. Each sample was successively passed through all the technical stages of the high temperature treatment used in the initial fabrication (Table I)

Table I - Technical Stages in Preparing the Detectors

I) The unprocessed materials.
II) Oxidation at 1000°C in a "wet" oxygen atmosphere with chlorine dopants for three hours to form a 0.6 μm thick oxide layer for the contact plates.
III) A repeat at 1150°C in a dry oxygen atmosphere for one hour to form a 0.2 μm oxide layer to separate the diodes.
IV) Boron diffusion at 1150°C in an oxygen-nitrogen mixture.
V) Annealing in a hydrogen atmosphere at 900°C for five minutes.
VI) Annealing in $H_2$ at 450°C for thirty minutes.

Fig. 20 shows the variation of resistivity and electron concentration for two wafers with starting resistivities in the range of 2 and 4 KΩ·cm, after each of the thermal treatment stages I - VI discussed above. Resistivity monitoring was done using the standard four-point method. A significant decrease of resistivity appeared after the V stage when the samples were annealed in $H_2$ at 900 °C. This was due to the appearance of new electrically-active centers with a concentration of approximately $10^{13}$ $cm^{-3}$.

Fig. 21(a, b) presents the results of DLTS measurements for the same samples after the high temperature treatments in stages II-VI. Each peak of the spectrum refers to one deep level. The

peak height characterizes the concentration of the level. The shape and the temperature peak position determine the level's ionization energy and electron capture cross section[30].

Six levels have been identified in the spectrum (designated by arabic numerals 1-6). The ionization energy (E) and electron capture cross sections ($\sigma_n$) for the levels are given in Table II:

Table II - Energy Levels Identified by DLTS

| Level | Ion. Energy (Ev) | Capture Cross Section ($cm^2$) |
|---|---|---|
| 1 | -0.16 | $6 \cdot 10^{-15}$ |
| 2 | -0.22 | $2 \cdot 10^{-14}$ |
| 3 | -0.26 | $3 \cdot 10^{-16}$ |
| 4 | -0.36 | $7 \cdot 10^{-14}$ |
| 5 | -0.44 | $4 \cdot 10^{-15}$ |
| 6 | -0.49 | $2 \cdot 10^{-16}$ |

The test results for the wafers before processing (stage I) indicated that the unprocessed material was rather free of deep-level centers. A single level observed in the wafer b spectrum (level #6 in Fig. 21) was due to a center with a concentration of $2 \cdot 10^{10}$ $cm^{-3}$. A comparison of the parameters for this with known silicon data suggests that the unprocessed material contained iron as a residual impurity at a concentration of less than 5% compared to the main doping impurity.

Several new levels appeared in the spectral analysis after each temperature treatment in stages II-VI. Nevertheless, their concentration remained negligible compared to the main dopant up to stage V. After stage V a new level appeared in all the wafers (level #2 in Fig. 21) with a concentration several times more than the dopant concentration. The appearance of this new level resulted in an abrupt decrease of the material resistivity. The concentration of level #2 is exactly equal to the increase of the electron concentration resulting from doping the a and b samples after the V stage.

It is known that atomic hydrogen cannot produce any kinds of deep levels in silicon. However, estimates show that none of the known impurities other than hydrogen can penetrate silicon to depths of 150 - 200 µm in 5 minutes at 900°C. This suggests that the level with $E_c$ = 0.22 eV is formed as a complex between hydrogen and an electrically inactive impurity contained in the starting material.

After the DLTS analysis revealed the impurity level problem the implantation technology was altered. The hydrogen anneal at 900°C was changed to a low temperature anneal in a nitrogen atmosphere. This prevented the creation of the centers that

decreased the resistivity of the material and significantly improved the volt-ampere characteristics of the detectors.

## 6. ALIGNING AND BENDING CRYSTALS

The bending device is an important element of high energy channeling experiments. At energies of hundreds of GeV the angular acceptance for capture into the channeling regime are on the microradian scale. Bending angles span the hundred microradians-milliradians regime. This means the bending device has to be precisely formed. The device is further complicated because it is necessary to take in to account different types of aberrations accompanying the crystal bending and try to compensate these effects.

The majority of bending devices being used can be schematically classified under two approaches to bending a crystal[31] (see Fig. 22).

The first approach (Fig. 22a) is called the "concentrated load P at the center" method or the three-point method of bending. The second one (Fig. 22b) is called the "couple M at the free ends" or moment (sometimes called the four-point) method of bending.

The shape of the plate is different for each case. For instance, the equation of the surface for the variant in (Fig. 22a) has the form:

$$y = (2\theta x^2/L)(1-2x/3L) \qquad (4)$$

where $\theta$ is the angle between the tangent to the curve at the point $x = L/2$ and the x axis, and L is the distance between the outermost points of the crystal support. For this shape of the plate, the radius of curvature changes substantially as a function of x.

$$R(x) = L^2/(4\theta(L-x)) \qquad (5)$$

The maximum sagitta $\delta$ at the crystal center is:

$$\delta = L\theta_0/3 \qquad (6)$$

For a bending angle of 1.65 mrad (the case for the E761 experiment) and L = 4 cm the maximum sagitta is equal to 11 µm and the radius is $R_{min}$ = 12 m.

For the variant shown in Fig. 22b the equation of the surface, the radius of curvature, and the sagitta are:

$$y = \theta x^2/L \ ; \qquad R = L/2\theta \ ; \qquad \delta = L\theta_0/4 \qquad (7)$$

For the E761 bending angle of 1.65 mrad, $\delta$ = 8.3 micrometers and R = 24 m for this variant.

These formulas are right in the approximation of the two dimensional case and an isotropic body. The situation is more complicated for the three-dimensional case particularly if the anisotropy of the elastic properties is taken into account. For example, for elastic bending of a crystal plate through a cylindrical curve of radius R with the moment method (Fig. 22b) the stresses are:

$$\sigma_z = S_{55}y/(R(S^2_{35}-S_{33}S_{55})) \quad (8)$$

$$\sigma_{xz} = S_{35}y/(R(S^2_{35}-S_{33}S_{55})) \quad (9)$$

$$\sigma_x = \sigma_y = \tau_{xy} = \tau_{xz} = 0 \quad (10)$$

where $\sigma_i$ is the normal component of stress, $\tau_{ik}$ are the shear components of stress and $S_{pl}$ are the coefficients of elasticity which characterize the anisotropy of the elastic properties of the crystal. The values of $\sigma_z$ and $\tau_{xz}$ depend on the orientation of the crystal structure relative to the crystal body and bending geometry as well as the type of elastic symmetry of the crystal.

For the orientation used in E761, these formulas give $\sigma_z >> \tau_{xz}$ and $\sigma_z = 512 \cdot y$ KG/cm$^2$ for R = 24 m. The maximum values occur at the crystal surface. At y = -T/2 (on the convex surface where T is the thickness) the crystal is stretched but at y = T/2 the crystal is compressed. The value for $\sigma_z$ for T = 0.4 mm is equal to ±10.2 KG/cm$^2$. This value is significantly less than the ultimate stress of silicon under compression[32], $\sigma^1_z$ < 947 Kg/cm$^2$. For the three-point bending scheme the value $\sigma_{zmax} \approx \pm 20$ Kgm/cm$^2$ is also significantly less than $\sigma^1_z$.

In addition the equilibrium shape of the entire plate can be different when one tries to achieve cylindrical bending as seen in Fig. 23. In particular it will depend on the topology of the (111) plane (see Fig. 24), the type of elastic symmetry of the crystal, and so on. This dependence depends on the sign and value of k[33], where

$$k = (S_{13}S_{55}-S_{15}S_{35})/2R(S^2_{35}-S_{33}S_{55}). \quad (11)$$

These are illustrated in Fig. 24:

This property of crystal elastic anisotropy is used in x-ray diffraction optics[34], but it may cause unwanted aberrations when it is used for channeling studies with bent crystals. Additional shape complications can arise due to finite plate dimensions, edge effects, and unrelieved forces and moments which are present in a real bending device. For example, in the Leningrad Nuclear Physics Institute GeV channeling experiment[35] the plate bent around a cylinder really had the more complicated shape at its ends shown in Fig. 25. When the bending angle of the plate was equal to 21.7±2.4 mrad for the edge faces it was α' = 9.4±0.3 mrad only.

Based on these considerations a three-point bending scheme was chosen for the E761 channeling experiment (see Fig. 22a). For this case the maximum tension and deformation occurs at the center of the plate and the minimum tensions are at the ends of the plate. This means that for the three-point scheme it is possible to have the minimum aberration at the ends of the plate. For the case of cylindrical bending there is a sharp change in the deformation state at the end and, correspondingly, the influence of edge effects increases.

It was important for E761 to separate the particles captured at the crystal edge from those trapped due to the volume capture effect[36]. With the three-point scheme this is easy to do because the initial portion of the plate is flat. In the case of uniform cylindrical bending these two types of channeling capture occur practically at the same part of the upstream end of the plate so that it is difficult to separate the two parts.

## 7. THE E761 BENDING SYSTEM.

The E761 bending device is shown in Fig. 26. This device has several principal parts including a support structure which holds the seven crystals, two remotely-controlled mechanisms to change the crystal bending angle for the upstream and downstream ends of the crystals, and a remotely-controlled goniometer that rotates the bending device around a horizontal axis.

Fig. 27 shows a plan view of the crystal support structure (2) as well as cross sections of the central and end parts. The three upper and three lower crystals were supported on precision 1.5 mm diameter steel balls (10) at the center part of the long edge of the crystals. In the experiment the upper and lower crystals were bent in opposite directions. This was aimed at the possibility of observing spin precession in opposite directions simultaneously. The ends of the crystals were separated from each other by small ball-bearings calibrated to 1 μm precision. These balls, which supported the ends of the crystals, were fixed by flexible steel plane springs (11). Through the movable pivots of the bending mechanism (7) in Fig. 26, a force pushed down on the ends of the crystals for the upper crystals and up for the lower crystals. The center crystal had a fixed support and did not bend like the other crystals so that it remained flat. Fig. 28 schematically illustrates the bending method. It was a typical three-point scheme of bending as illustrated in Fig. 22a so that the shape of the bent plate is a cubic parabola. The points of contact on the plate are also shown.

The location of the terminals for the connections of the detector signal outputs (13) and the high-voltage inputs (14) is shown in Fig. 16.

The mechanisms to change the crystal bending angles ((4) in Fig. 26) were precise, sophisticated devices which provided smooth motion of the bending pins (7) in the 0-80 μm range. This provided a smooth variation of the bending angles for the end parts of the crystals over the 0-4 mrad region. DC motors (8) were used for remote control of the crystal bending. A 20-turn potentiometer (9) tightly coupled to the motor axis indicated the motor state. Fig. 29 shows the relations between potentiometer voltage and the bending angles for upper and lower crystals for the upstream (Fig. 29a) and downstream ends (Fig. 29b) of the crystals.

The requirement for separate bending devices for the upstream and downstream parts of the crystal was caused by the specific geometry of the E761 experiment. The angular orientation of the upstream ends of the crystals was related to the distance from the production target to the upstream edges of the crystals. As a result it was necessary to orient the front ends of the crystals so they pointed at the target (see Fig. 30a). For example, the

goniometer position along the beam established a requirement that the upstream edges of the 2nd and 5th crystals be oriented several hundred microradians away from the nominal beam center line. Because of the uncertainty of the crystallographic plane alignment with the crystal surface (< 500 μrad) a large dynamic range (4 mrad) was provided to cover the possible bending required. In addition, uncertainty in the plate orientation inside the bending device could also be significant so additional bending dynamic range was required.

A similar situation held for the downstream ends of crystals (see Fig. 30b). The deflection angle which could be used was about 1.5 mrad, set by the requirement that the deflected beam had to pass through a 67 mm vertical hole in the E761 electromagnetic calorimeter (BGO/LG in Fig. 1). Because of the possible crystal orientation uncertainties, each of the three crystals in the upper or lower arrays had the same bending angle.

A two-crystal x-ray diffraction spectrometer geometry was used to orient the crystals before the experiment. Fig. 31 shows the x-ray spectrometer scheme used to align the six bent crystals relative to the central plane crystal. This spectrometer also measured the curvature of the bent crystals.

Fig. 31 shows a side view of the x-ray spectrometer. An x-ray source with a silver anode was used. The characteristic $K_\alpha$ line for this anode has a wavelength of 0.5591 Angstroms. The collimator hole was 15 mm high by 7 mm wide. The entire goniometer bending array was placed at the normal location of the first crystal in a two-crystal spectrometer. A 6 mm portion along the crystal (for any of seven crystals) was used as the crystal-monochromator. This region was selected by using a slit collimator 0.5 mm high just after the crystal array in the goniometer and by vertically shifting the whole bending array. Bragg diffraction off the (111) planes was used. The same (111) planes were also used for the channeling experiment.

The diffracted beam which passed through the slit fell on the crystal-analyzer which was attached to the goniometer. The diffraction angle could be measured with a precision of 2.5 μrad using the goniometer. The (111) plane was also used as the Laue-reflection plane for the crystal-analyzer. For this case a two-crystal spectrometer has no dispersion and the width and shape of the diffraction line depends only on the conditions for diffraction. After reflection from the crystal-analyzer the diffracted beam fell on an x-ray detector.

When a plate was bent in the bending device the reflecting (111)-planes changed their orientation relative to the (111) planes in the crystal-analyzer. A typical diffraction line is shown in Fig. 31b. This is a case where the angular position of the edge of one of the crystals was illuminated by the slit. The sharp edge of

the diffraction line is determined by the angular position of the plate edge under study. The width of the line results from the curvature of the portion of the bent crystal that was illuminated with x-rays. By determining the angular orientation of the crystal edges the crystals were installed inside the bending device with the correct nominal initial bending and inclinations for both the upstream and downstream ends of the crystals.

For the dimensions of the crystals used in this experiment, the bending scheme shown in Fig. 25-27 did not compensate for aberrations in shape and the magnitude of the bending in different regions of the crystal plate. The program ANSYS 4.4A was used to exactly simulate the geometry used for bending. The ANSYS calculations showed that these aberration were small for the E761 case. Fig. 32a is a three-dimensional view showing the ANSYS calculation for a crystal plate with the E761 bend angle of 1.5 mrad. The shape of the bent plate is not exactly a cubic paraboloid. Due to the finite plate dimensions the distribution of stress (in MPa) shown in Fig. 32b is more complicated. Note that the crystals in the E761 experiment were two orders of magnitude away from serious strain problems. Fig. 33 shows two (XY) cross-sections of the plate based on the ANSYS calculation for the upstream end and the mid-section. Note that most of the change of curvature comes from the middle section. From Fig. 33 it is possible to estimate the magnitude of the non-cylindrical behavior in these parts of the plate. The bending angle in the YZ-plane ranges from 1.5 mrad in the middle part of the crystal plate to 1.618 mrad at the edges of the plate. The angular resolutions of the E761 spectrometer system were good enough to observe the inhomogeneous nature of the crystal curvature. This could be seen as both a change of the deflection angle and angle of capture to the channeling regime for different X values across the crystal face. Because the average value of the deflection angle was large (1.6 mrad) in comparison with the width (70 μrad) of the outgoing angular distribution observed in the experiment. Since this width is observed using the integral of the particle distribution through X there was no significant influence on the average spin precession angle.

The crystals used for the E761 channeling experiment exhibited a behavior like that expected for a twisted crystal. Practically, the channeling angle in the y direction, TY1(channeled), changed with position across the front edge of a crystal (x in the E761 coordinate system).

There is nothing mysterious about this behavior. While the major faces of the crystals lay approximately in the x-z plane, no special effort was made to assure that they were perfectly level. Indeed there was no way to independently level individual crystals other than through delicate shimming. During the run uneven shims were introduced in the systems that could have easily caused "twists" at the level we observed.

"Twist" is used with some reservation here because misalignment in the x-y plane could also have been called a rotation. However it is also possible to have actual distortions in the crystal as seen in Fig. 32. For example, the bend itself is just that, a curl around the x axis. Again there is no reason to believe that a screw-like twist couldn't have been introduced in the crystal because of the nature of the shimming. This would result in the deflection angle (DTY below) changing with x. As noted earlier, there is also curvature in the x-y plane because of the six-point suspension used to bend the crystal.

Because of the fine spatial and angular resolution of the E761 spectrometer it was relatively straight-forward to measure these twists. This was done using the very large number of long-lived channeling events collected during the run. This had to be done carefully because of the possibility that aperture cuts for the overall system might bias the corrections. Such aperture cuts could arise both from the crystal channeling requirement and the E761 spectrometer.

Channeled particles were selected with an energy loss cut on the interval $0.55 < E < 0.85$ where E is the fraction of the most probable random energy loss for both the first and the last active pads on a crystal. In addition, a y cut was used to select the fully-depleted region of a crystal.

The TY1 angular distributions for the channeled particles were examined for 8-10 segments in x. Several fitting techniques were used including straight averages and gaussian fits. The maximum differences between the gaussian and RMS fits was 5 microradians.

The distribution of TY1 vs x was fitted using these techniques. As seen from Fig. 32, there is no reason to believe the twist fit should be linear.

Fig. 34 shows the entrance angles (TY1) across the crystal for the upper crystal. The simulation results in Fig. 33 shows that most of the saddle curvature (in the z direction) comes in the middle of the crystal. One can infer from this that the maximum change in TY1 along the front edge of the crystal in the active interval of 4 mm should be less than 4 microradians so that the remaining part is due to twist-like effects. The overall change in curvature along the crystal as a function of x amounts to 9.5% or 90 microradians. The maximum change as a function of x over a 4 mm active region in x is about 40 microradians.

The DTY distribution should exhibit more curvature. The total amount of variation as a function of x depends on the x location. At the center of the saddle the ANSYS program gives a variation of about 4 microradians for an x interval of 0.4 cm. For the maximum curvature case the variation is 40 microradians in the same interval. Fig. 35 shows the variation of DTY for the upper crystal

including linear and quadratic fits to the points. The ANSYS simulation, adjusted to place the minimum curvature at x = 2.05 cm, is also shown. Both the #2 and #5 crystal linear fits are consistent with the simulation.

## 8. SUMMARY

These technical studies for the E761 channeling spin precession experiment have led to a number of new insights. This experiment was one of the first channeling experiments to employ multiple crystals. For the first time sophisticated pre-alignment schemes were used to set crystal bending angles and orientations using x-ray diffraction techniques. New tools were developed for the studies of defects in channeling crystals. Dechanneling from dislocation slip planes was observed for the first time. New insights were gained concerning techniques for implanting detectors on channeling crystals. System spatial and angular resolution was good enough to observe crystal distortions and see their impacts for the first time.

The experiment has shown that sophisticated technical and crystal quality issues can be solved for channeling applications in the TeV range. It has also pointed the way to investigating these issues at levels required for channeling applications in the 10 TeV regime prior to the availability of beams.

The authors would like to thank their colleagues in E761 for their assistance and for many discussions. We would also like to thank members of the SSC Super Fixed Target (SFT) proposal (SSC EOI-14) and the associated Fermilab experiment E-853 as well as a number of channeling experts at Serpukhov and CERN for many fruitful discussions. We thank the staffs of Fermilab and the Petersburg Nuclear Physics Institute for their assistance. T. Nicol of Fermilab carried out the ANSYS calculations.

This work was supported in part by the U.S. Department of Energy under contracts DE-AC02-76CH0300 and the Russian Academy of Sciences.

+ Deceased

REFERENCES:


1. R. Carrigan, p. 339, **Relativistic Channeling**, eds. R. A. Carrigan, Jr. and J. A. Ellison, Plenum, New York (1987).

2. H. Akbari, et al., Physics Letters, **B313**, 491 (1993).

3. A. S. Denisov, et al., Nucl. Instr. and Meth., **B69**, 382 (1992).

4. S. I. Baker, et al., Nucl. Instr. and Meth., **A248**, 301 (1986).

5. D. Chen, et al., Phys. Rev. Lett. **69**, 3286 (1992).

6. Invited paper by K. Lau, "The Super Fixed Target Facility at the SSC", S. E. Anassontzis, et. al., Third Topical Seminar on Heavy Flavours, San Miniato, Italy (1991).

7. R. A. Carrigan, Jr., et al., ICACS A19 (1993), to be published in Nucl. Instr. and Meth.

8. V. V. Baublis et al., Proceedings of the 15th International Conference on Atomic Collisions in Solids, B15 (1993), to be published in Nuclear Instruments and Methods.

9. E. N. Tsyganov, Fermilab TM-682, Batavia, (1976).

10. V. G. Baryshevskii, Pis'ma Zh. Tekh. Fiz. 5, 182 (1979), Sov. Tech. Phys. Lett. 5, 73 (1979).

11. L. Pondrom, private communication and **Proc. of the 1982 DPF Summer School on Elementary Particle Physics and Future Facilities**, p. 98, eds. R. Donaldson, R. Gustafson, and F. Paige, Snowmass, CO (1982).

12. V. L. Lyuboshits, Yad. Fiz. 31, 986 (1980) [Sov. J. Nucl. Phys. 31, 509 (1980)]

13. I. J. Kim, Nucl. Phys. **B229**, 251 (1983).

14. A. Morelos et al., Phys. Rev. Lett. **71**, 2172 (1993).

15. M. Foucher et al., Phys. Rev. Lett. **68**, 3004 (1992).

16. A. Morelos, et al., Phys. Rev. Lett., **71**, 3417 (1993).

17. J. Lach and L. Pondrom, Ann. Rev. Nucl. Part. Sci. **29**, 203 (1979). L. Pondrom, Phys. Rep. **122**, 57 (1985).

18. Dong Chen, Ph.D. Thesis, State University of New York at Albany, 1992 (unpublished).

19. J. Lindhard, K. Dan. Vidensk. Selsk. Mat. Fys. Medd. **34**, 14 (1965).

20. V. V. Baublis, et al., Int. Conf. on Atomic Collisions in Solids, Western Ontario, Abstract 01, (1993), to be published in Nucl. Instr. and Meth.

21. T. S. Moss and S. P. Keller, **Handbook on Semiconductors-v.3, Materials, Properties and Preparation**, Elsevier Science Publishers, 1980, p.269-284.

22. V. Samsonov, p. 129 **Relativistic Channeling**, eds. R. A. Carrigan, Jr. and J. A. Ellison, Plenum, New York (1987). See also V. M. Biryukov, M. D. Bavizhev, and E. N. Tsyganov, SSCL-N-777 (1991).

23. H. Kudo, Phys. Rev. **B18**, 5995 (1978). See also V. M. Biryukov, M. D. Bavizhev, and E. N. Tsyganov, SSCL-N-777 (1991).

24. B. B. Loginov, L. A. Maslennikov, N. I. Tisnek, "High Purity Silicon Quality Investigation for Thermal Treatments Typical for PCCD Fabrication." Electronic Technique, Ser. 4, No. 1, (132) 3, (1991). (In Russian.)

25. V. V. Kuryatkov, et al., "Thermostability of High Purity n-Si During Planar Technology Operations," Electronic Technique, 1, (1992). (In press, Russian.)

26. See, for instance, **Ion Beam Handbook for Material Analysis**, Eds. J. W. Mayer and E. Rimini, p. 102, Academic Press, New York (1977).

27. D. Hull, **Introduction to Dislocations**. Atomizdat, p. 56 (1968).

28. V. J. Lang, Appl. Phys., V. **454**, no. 7, 3023 (1974).

29. Yu. V. Kuryatkov, Yu. V. Tuboltsev, preprint LNPI N1257, Feb. 1987. (In Russian.)

30. G. L. Miller, P. V. Lang, L. C. Kimerling. Ann. Rev. Matter. Sci. 1977, p. 377.

31. Timoshenko and MacCullough, **Elements of Strength of Materials**, 3rd ed., 182-183, Van Nostrand, Princeton, N.J., 1957.

32. See, for example, J. R. Patel and A. R. Chaudhuri, Journal of Applied Physics, **34**, 2788 (1963).

33. V. M. Samsonov, Leningrad Institute of Nuclear Physics, Preprint No. 278 (1976). W. Beer, P. F. A. Goudsmit, L. Knecht, NIM **219** 322 (84).

34. V. M. Samsonov and E. G. Lapin, Leningrad Nuclear Physics Institute, Preprint No. 587 (80).

35. V. M. Samsonov, Thesis (85).

36. O. I. Sumbaev, p. 117, **Relativistic Channeling**, eds. R. A. Carrigan, Jr. and J. A. Ellison, Plenum, New York (1987).

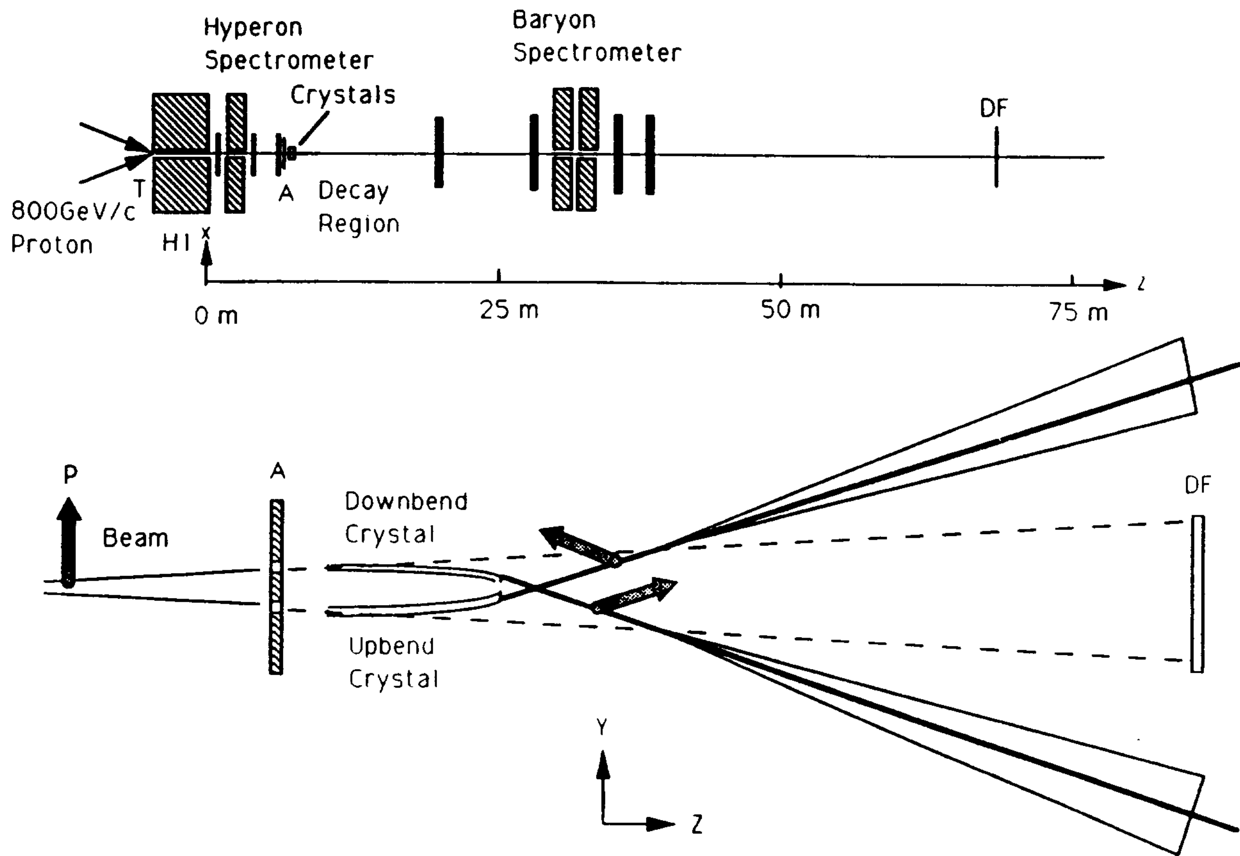


Fig. 1. Elevation schematic of the channeling apparatus. The arrows illustrate the spin precession in the crystals. Shaded areas show the $\Sigma^{+}$ decay cone. Straight-through particles strike the deflection anti, DF. The inset shows a plan view of the overall beam and spectrometer system.

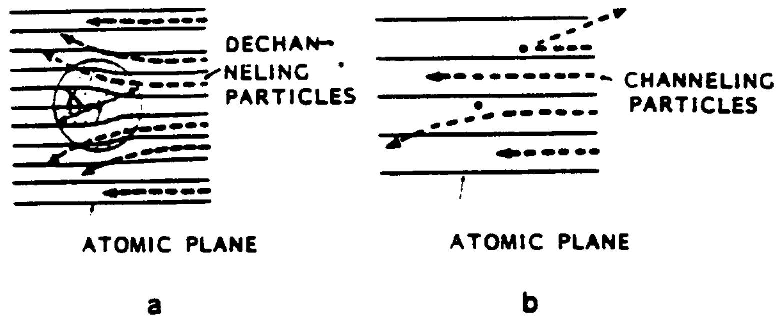


Fig. 2. Diagram of scattering and dechanneling processes for particles traveling nearly parallel to the atomic planes: a) on dislocations and b) on an impurity atom.

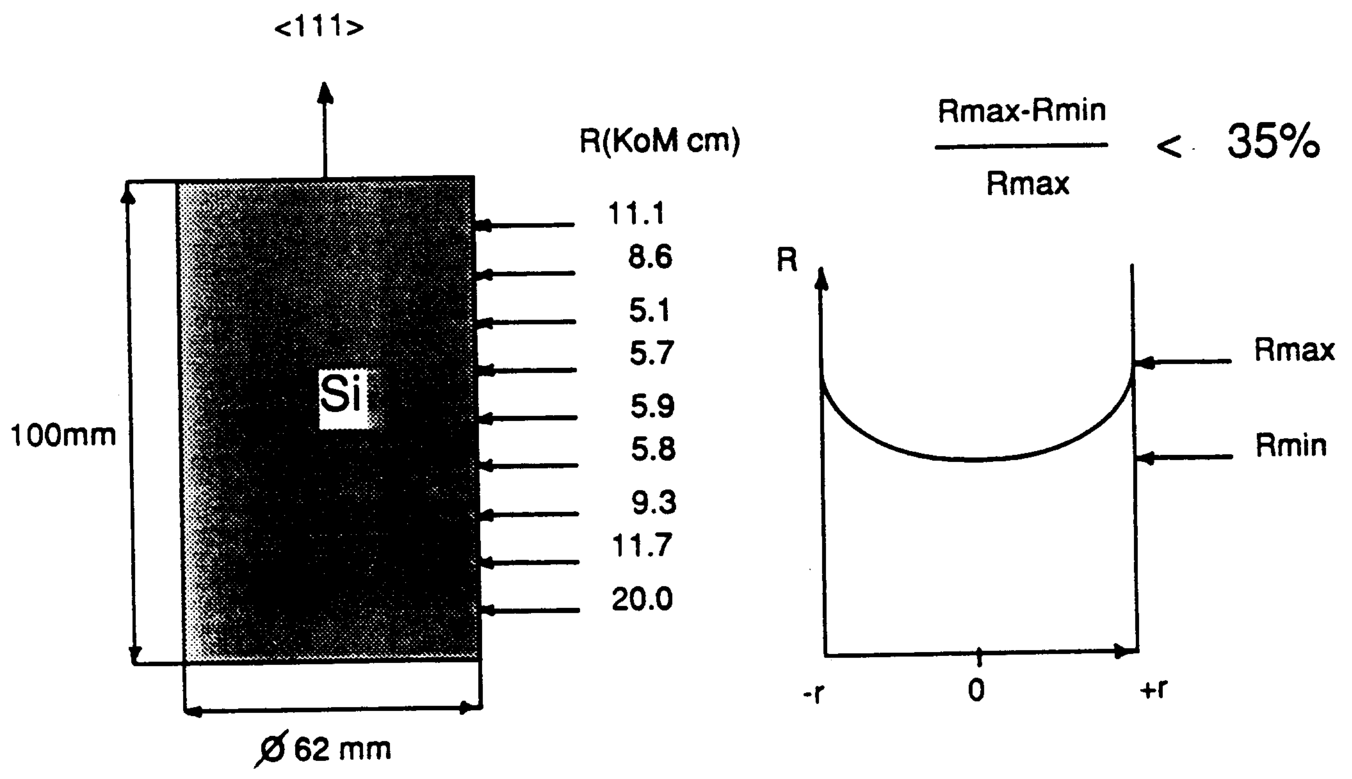


Fig. 3. Variation of resistivity over a typical silicon starting boule.

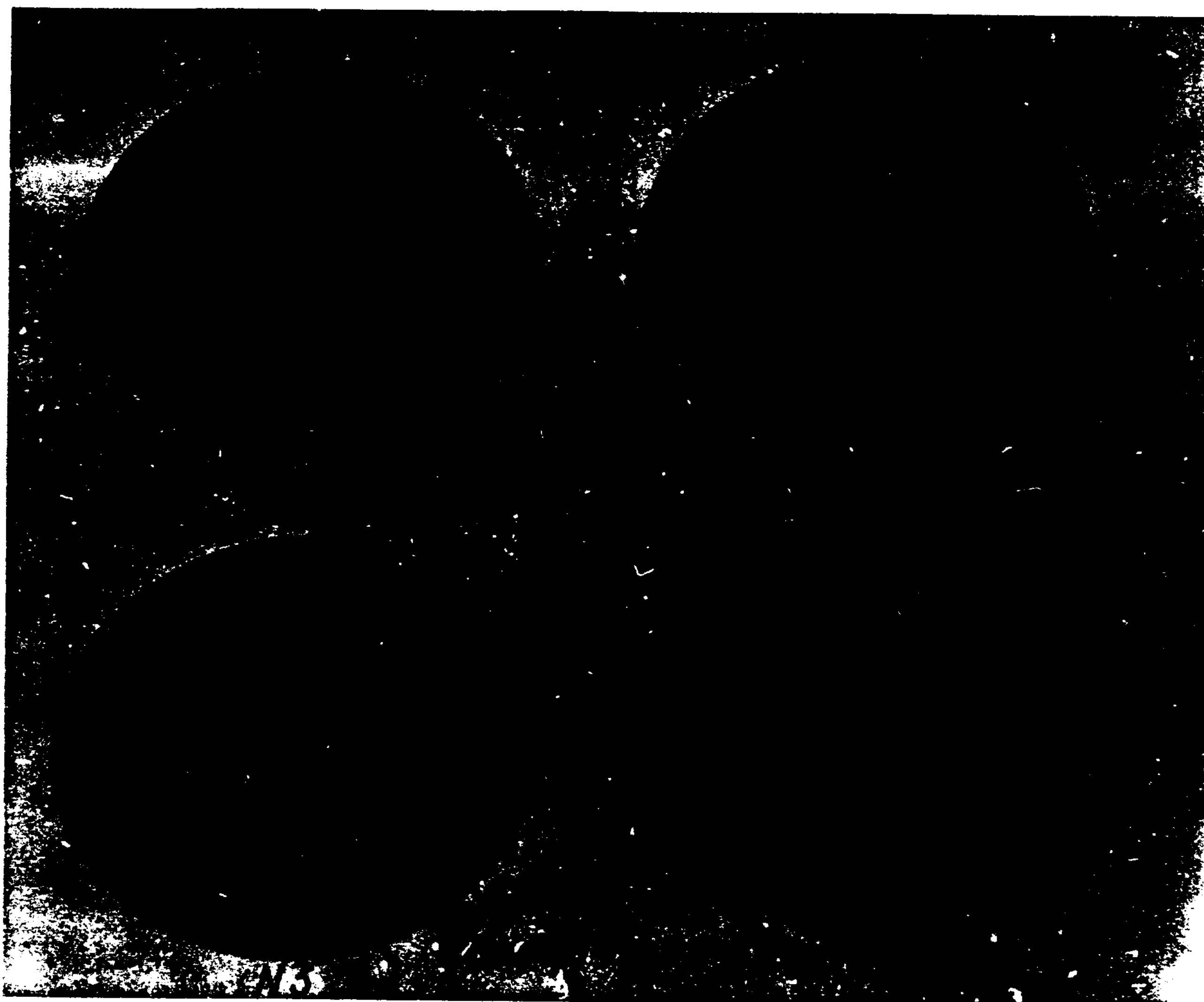

Fig. 4. Results from Si-H film decoration of four starting silicon wafers.

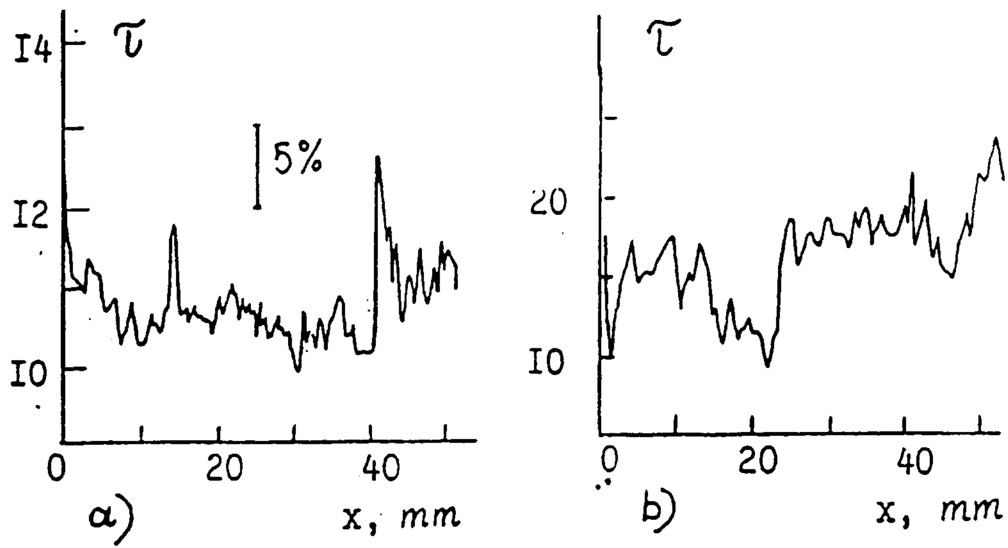


Fig. 5. Distribution of effective carrier lifetime (in arbitrary units) along a diameter for a) wafer N3 and b) N4 measured by SHF profiling.

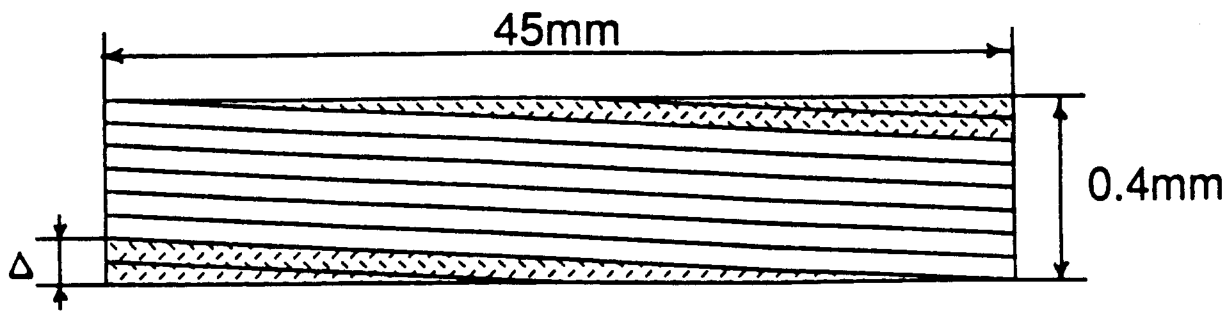


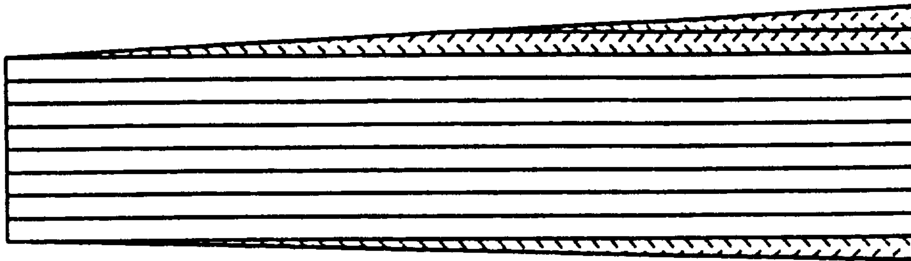


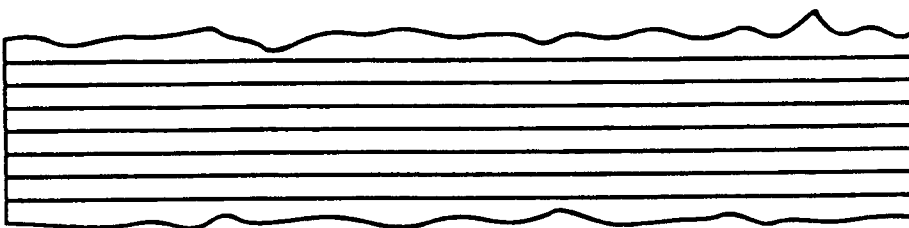


Fig. 6. Illustration of the effect of mis-aligning the body surfaces of the crystal relatives to the planes. a) Mis-orientation of the planes ($\theta = \Delta/45$ mm), b) the effect of thickness variations, c) the impact of surface roughness.

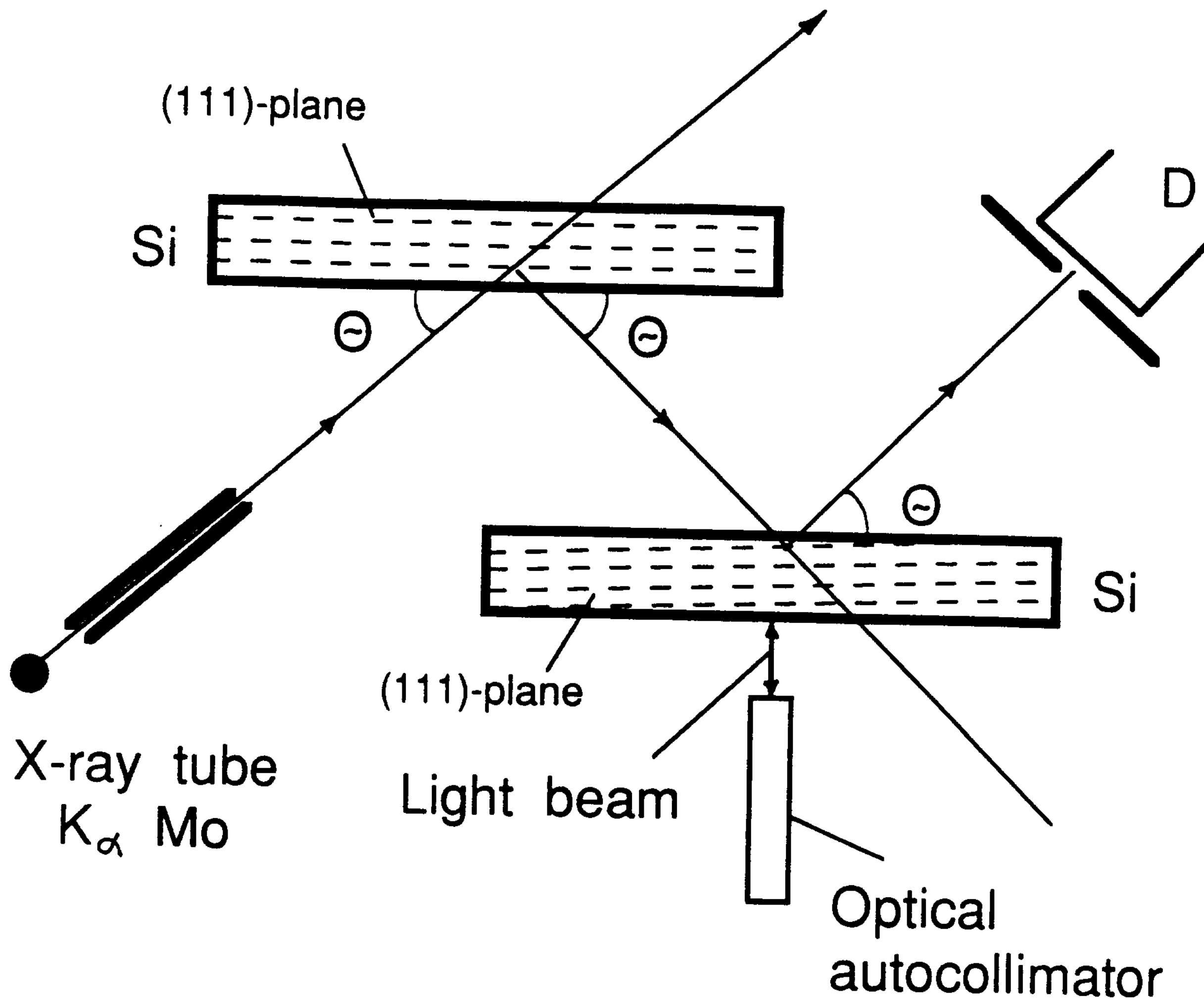


Fig. 7. Two-crystal diffraction spectrometer to improve the accuracy of the measurement of the angle between the crystal surface and the crystal and achieve a smaller value for the angle Δ and better surface parallelism.

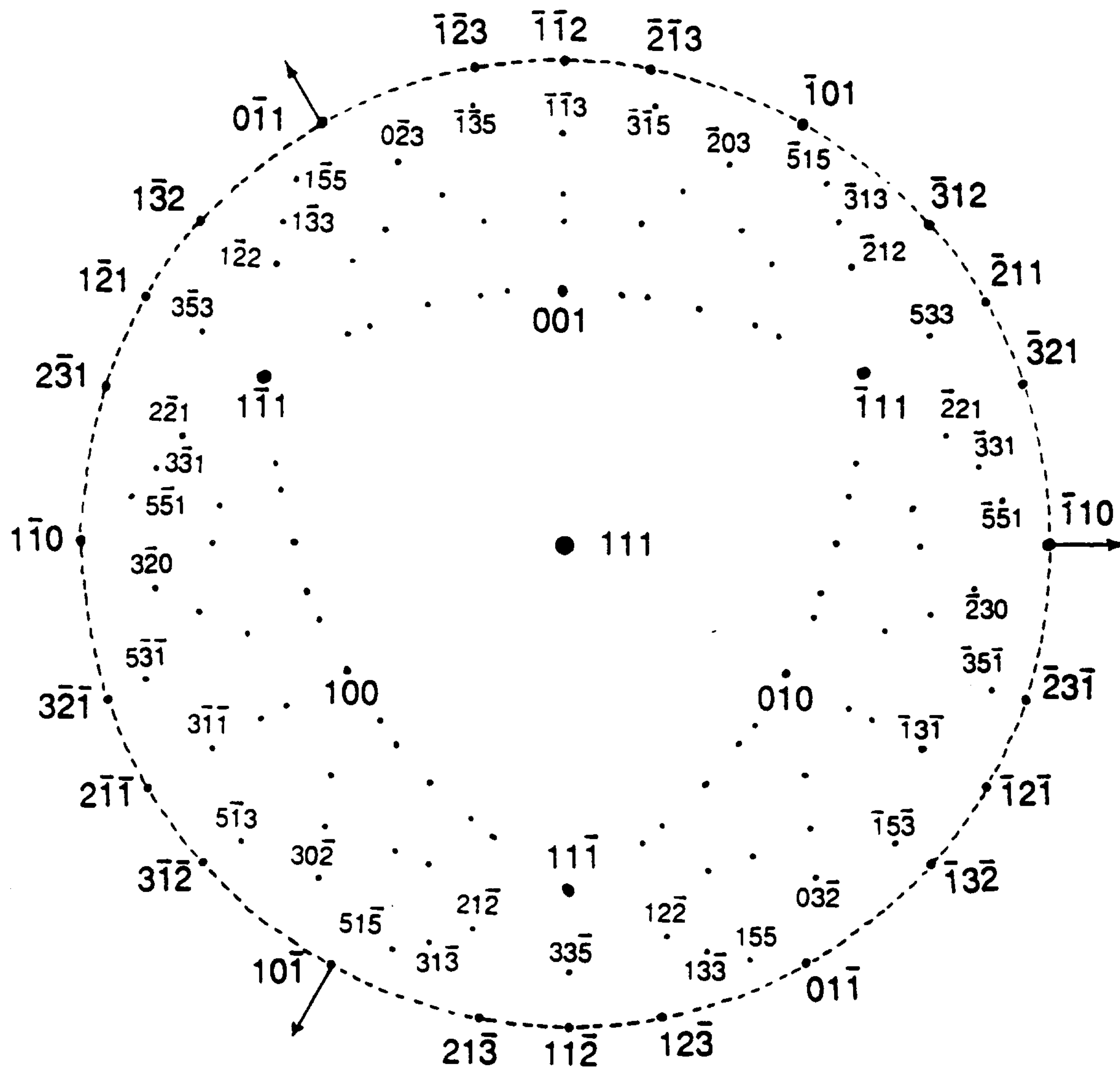


Fig. 8. Map of the stereographic projection of the intersections of different low index crystallographic axes (corresponding to the intersections of the crystallographic planes perpendicular to these axes) on the (111) plane and inside of a 15 degree limit relative to the (111) plane.

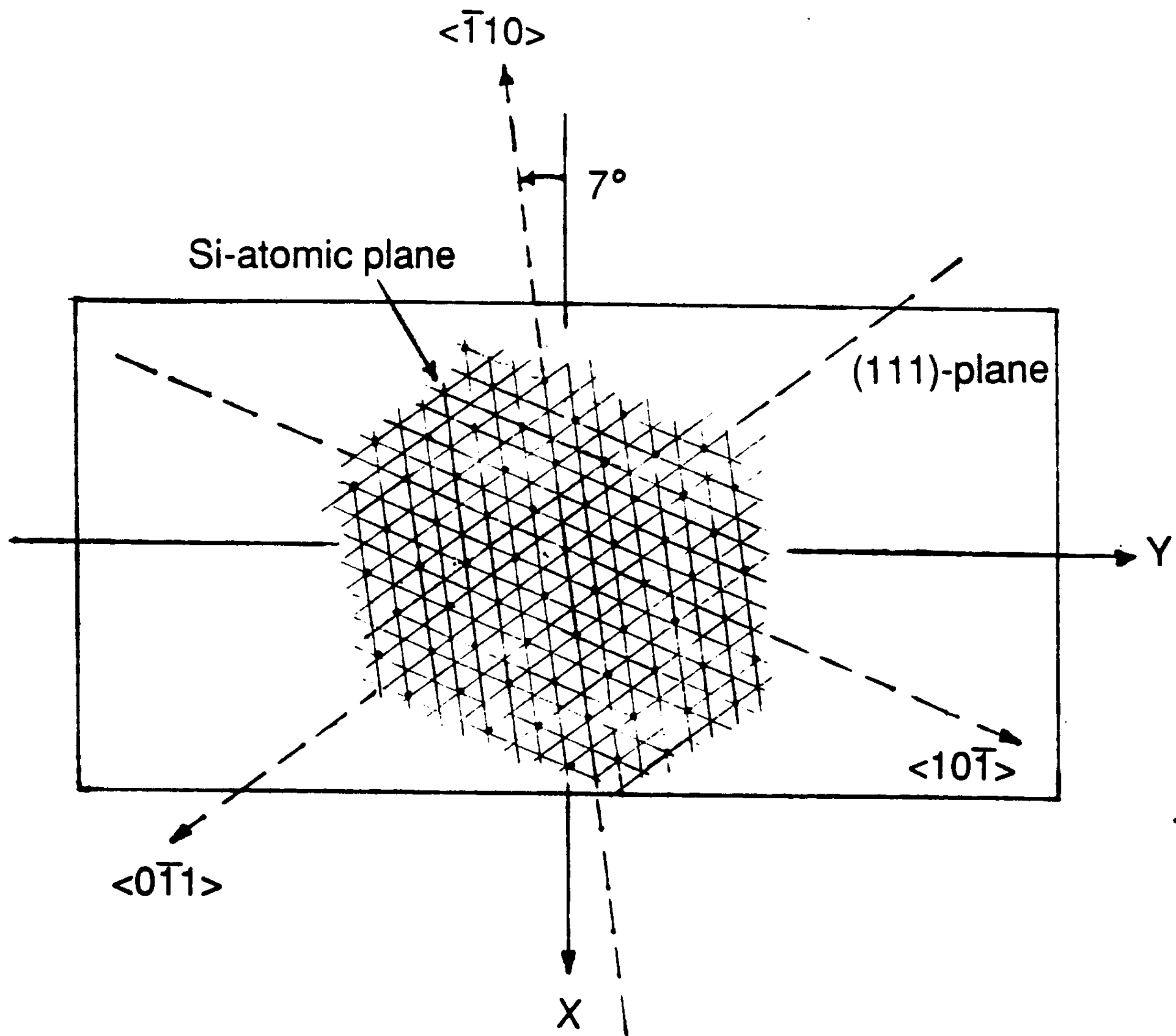


Fig. 9. Orientation of the E761 crystals. The long face was cut in a direction rotated 7 degrees to the ‹110› axis. A fragment of the atomic lattice in the (111) plane relative to the edges of the plate is also shown.

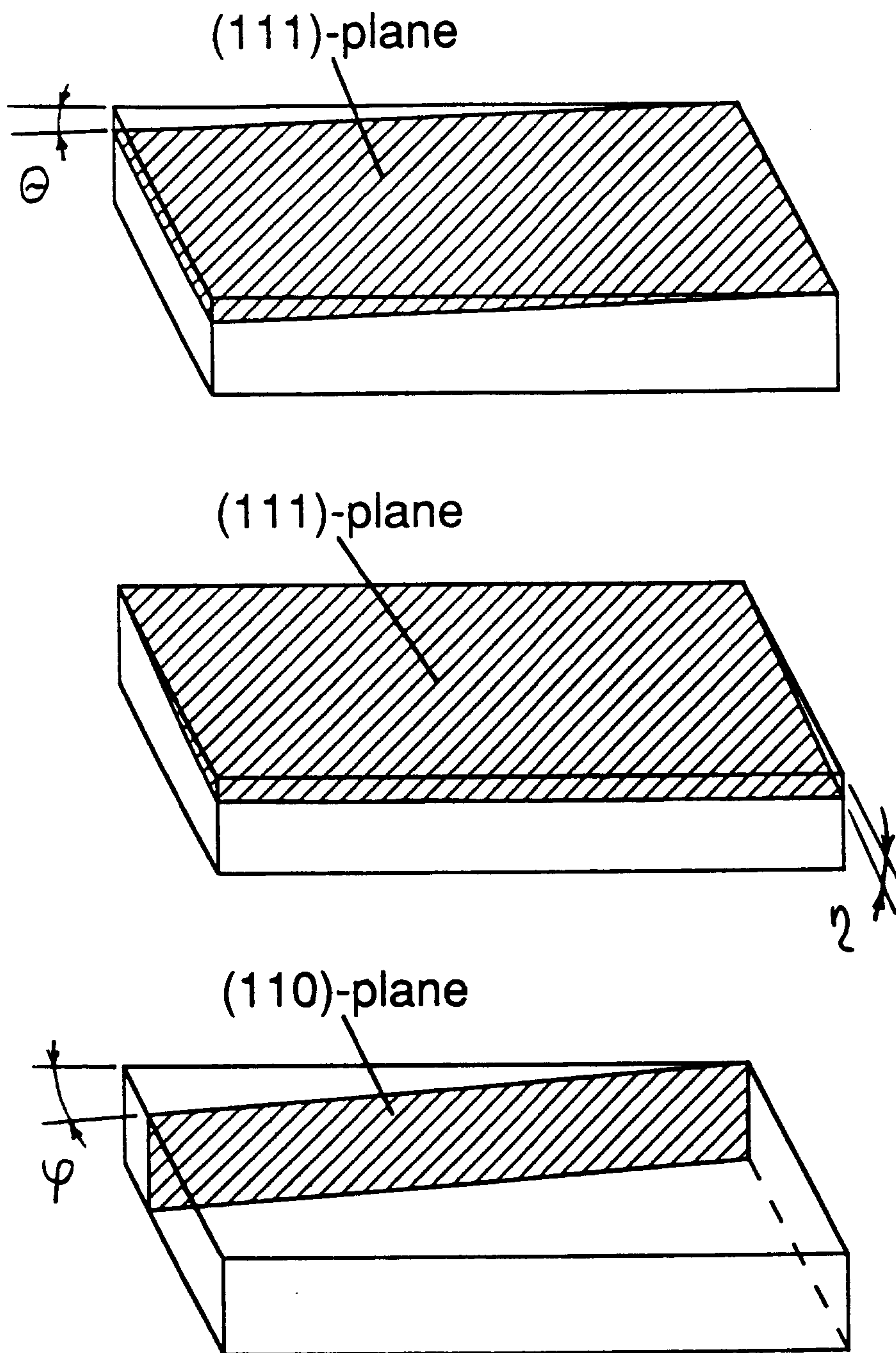


Fig. 10. Parameters for the crystallographic plane orientation for the E761 experiment.

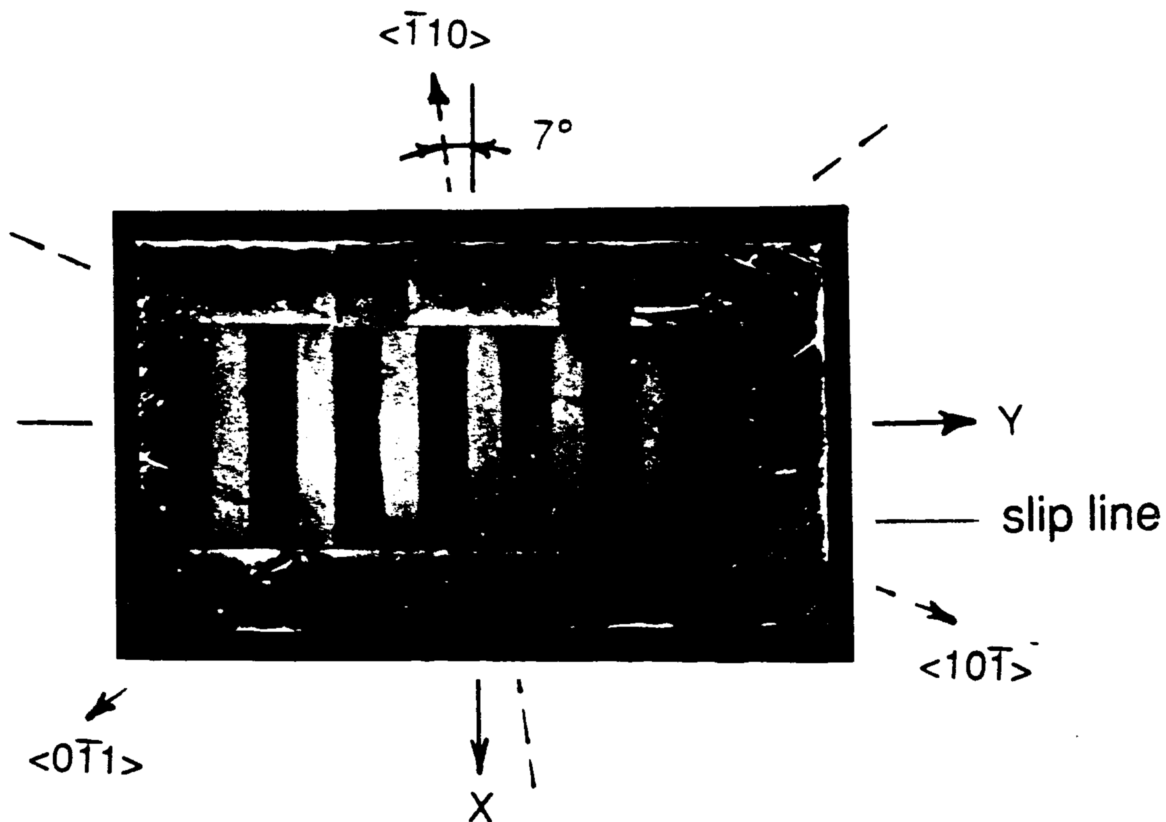


Fig. 11. Photograph of the Si-H films grown on the surface of a crystal after chemical etching of a 30 μm thick layer. The films reveal such structure defects as foliation and slip lines.

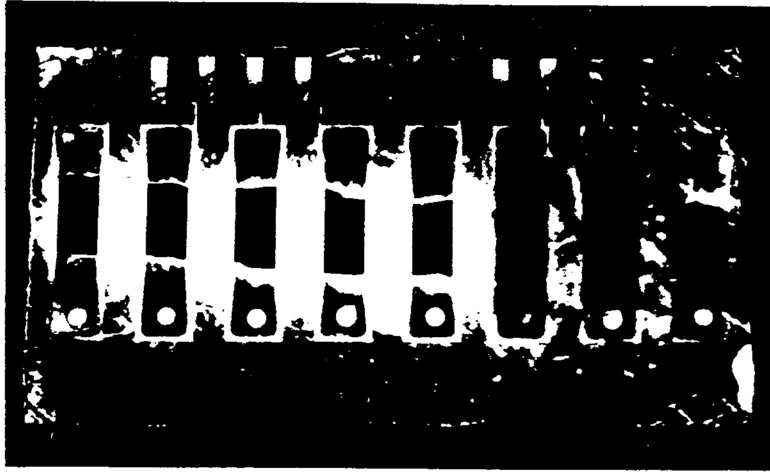

Fig. 12. Photograph of the crystal shown in Fig. 11 after etching the crystal and decorating with the Si-H film.

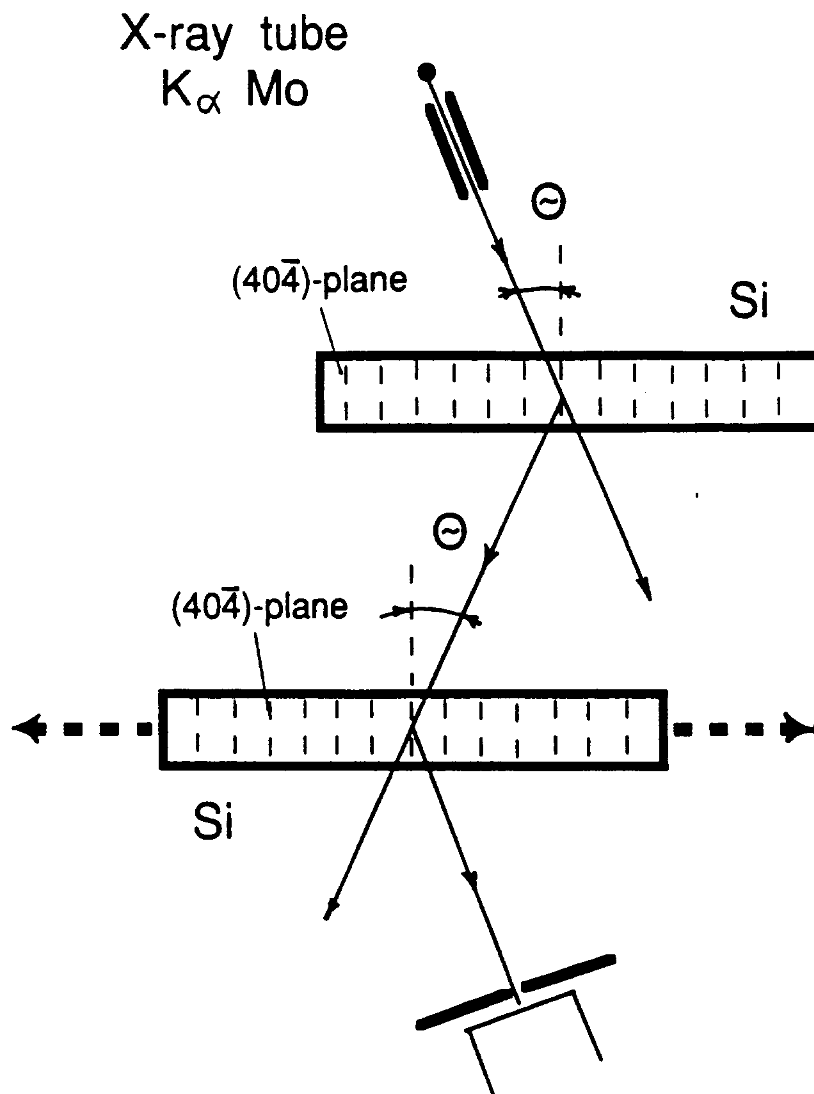


Fig. 13. Two-crystal diffraction spectrometer geometry used to confirm the crystal structure distortion in one of the E761 crystals. The E761 crystal was used as the analyzer in the two-crystal spectrometer. The Laue-Laue spectro-meter was tuned for diffraction from the (404) plane. The diffraction line width was then measured at different points along the crystal as the plate was shifted parallel to the E761 crystal.

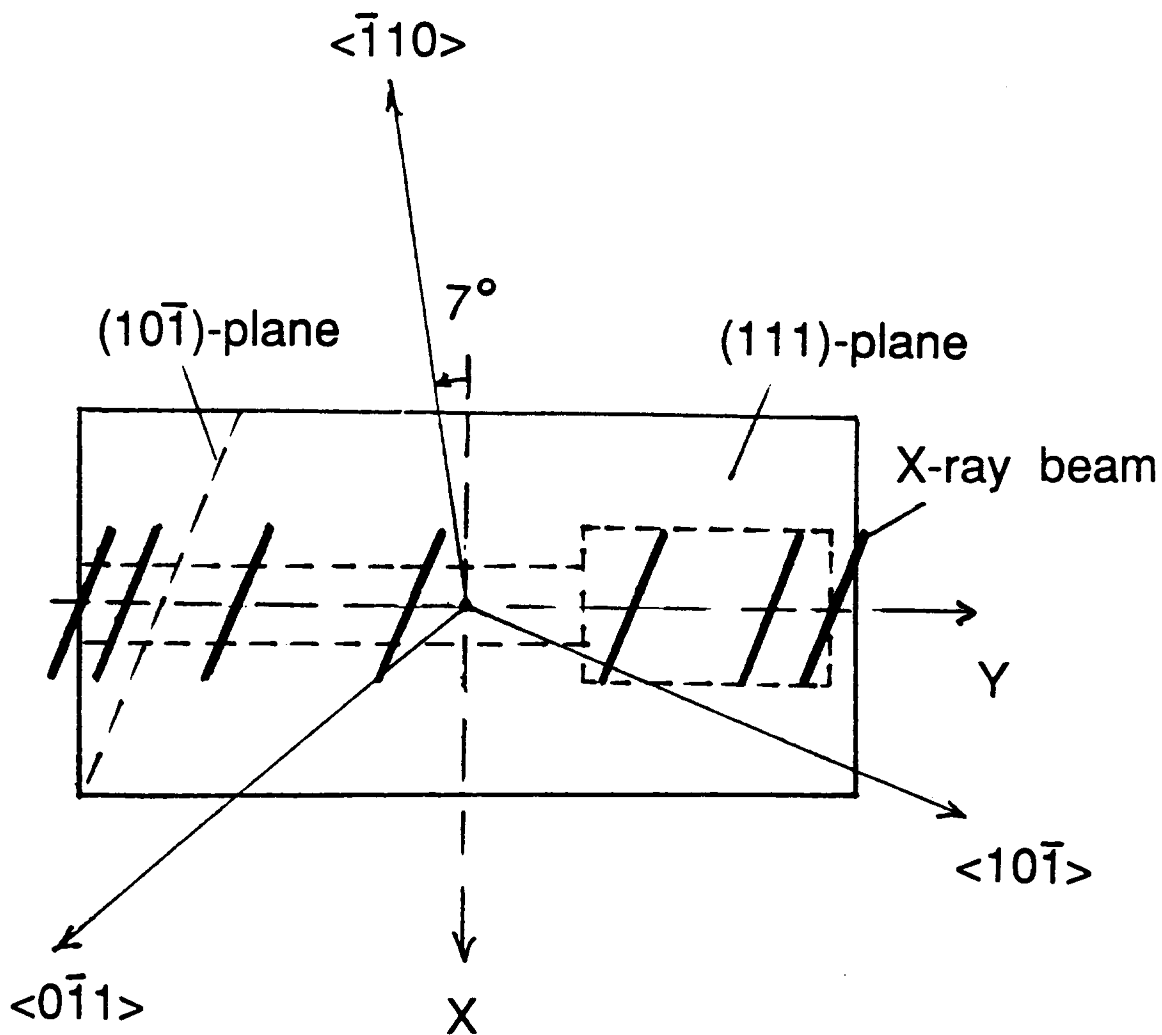


Fig. 14. Diagram showing the exposed regions of the E761 crystal (compare to Fig. 12). The solid lines show the crosssection of the x-ray beam on the surface of the plate.

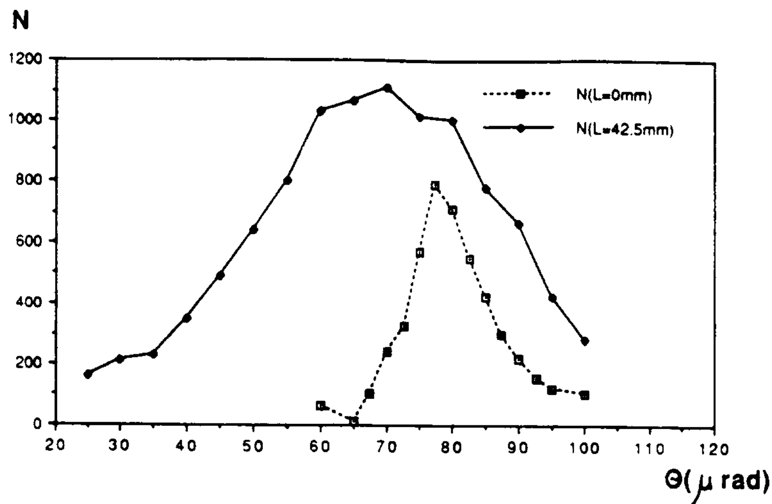


Fig. 15. a) Two-crystal spectrometer lines for two positions of the x-ray beam on the crystal surface (L=0, upstream; L=42.5 mm, downstream).

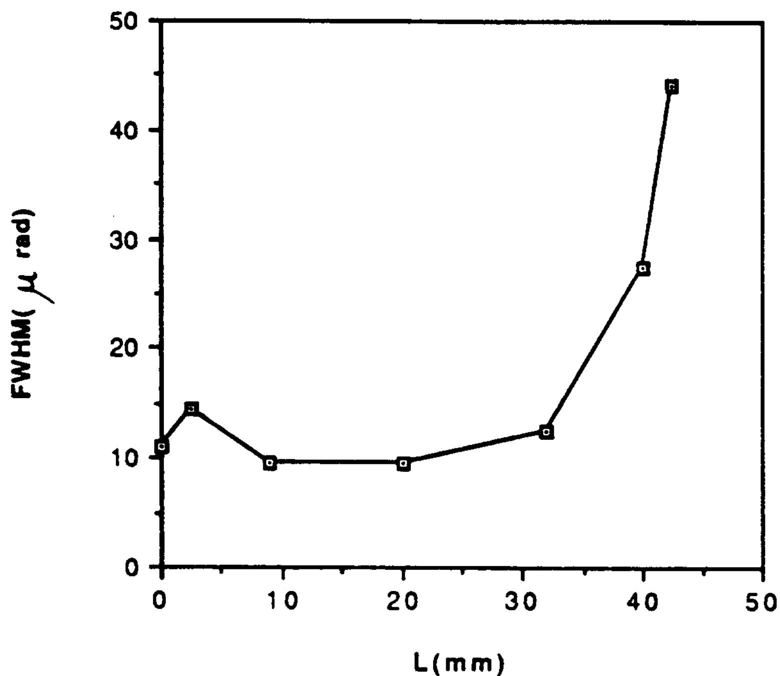


Fig. 15. b) The width (FWHM) of the two-crystal line measurements for all measured x-ray positions on the crystal surface. The diffraction peak in the region of L=30-45 mm (pads 6-8) is about four times wider than in the upstream portion of the crystal.

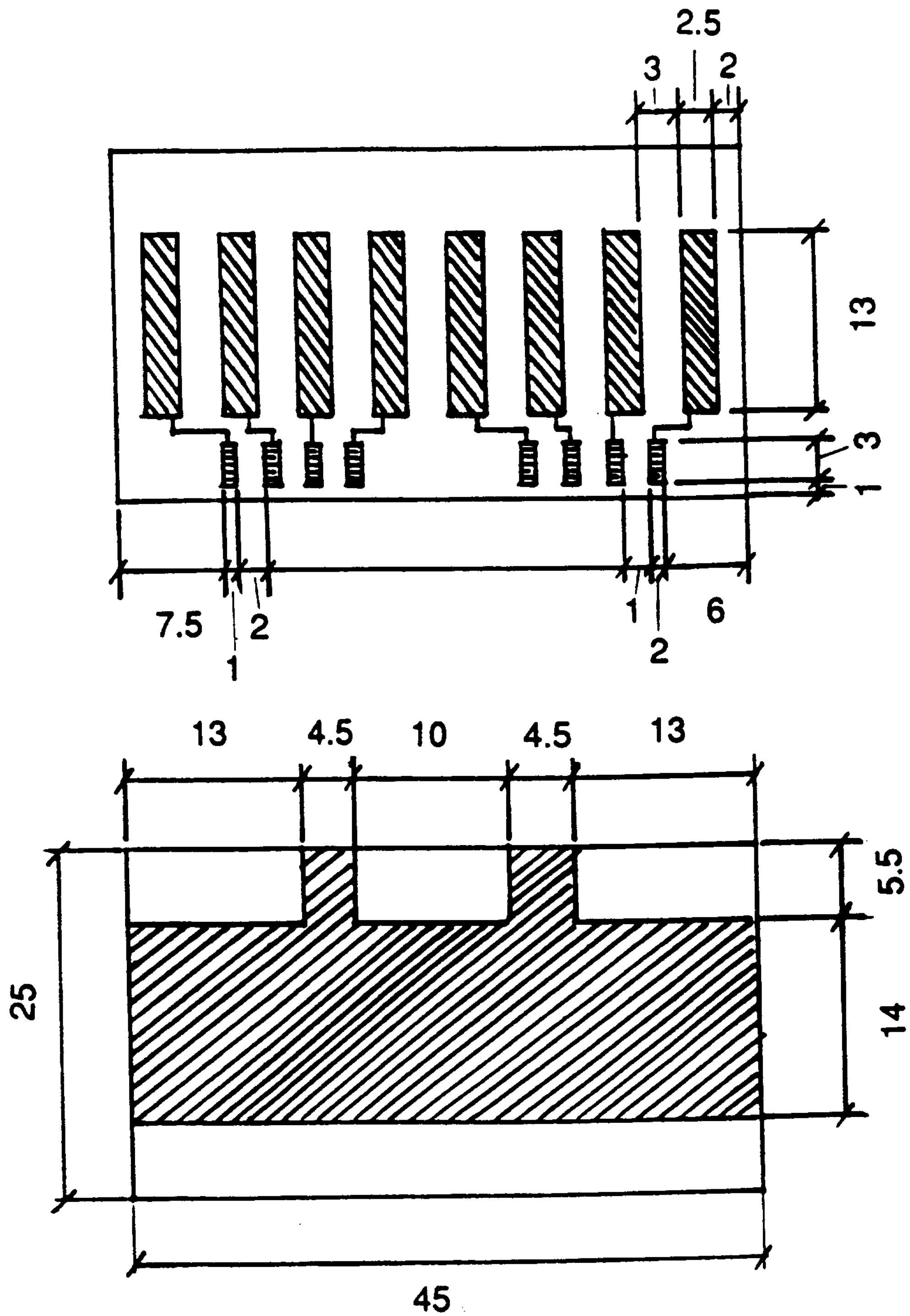


Fig. 16. Schematic layout of the E761 detector array. The array consisted of eight sensitive elements, each with an area of 2.5x13 $mm^2$ and with a 3 mm separation between each of the pads. The array was fabricated on a 45 * 25 $mm^2$ slice of silicon.

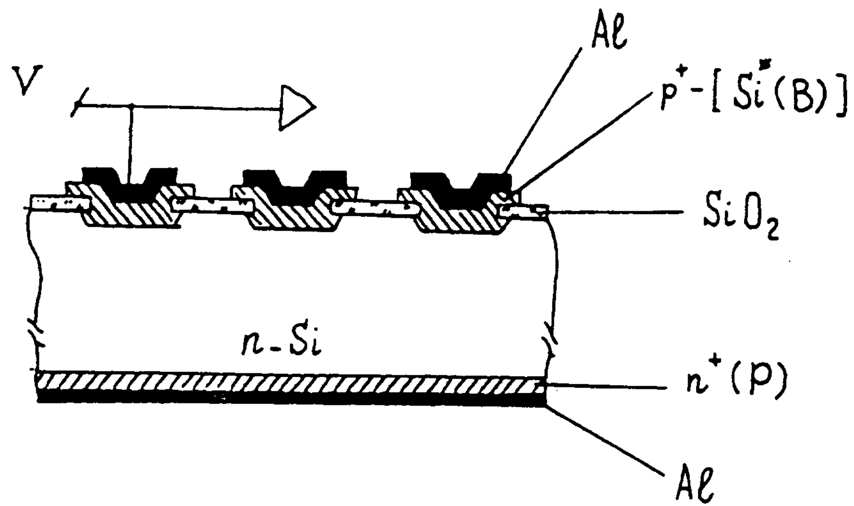


Fig. 17. Cross-section of the E761 implanted detectors.

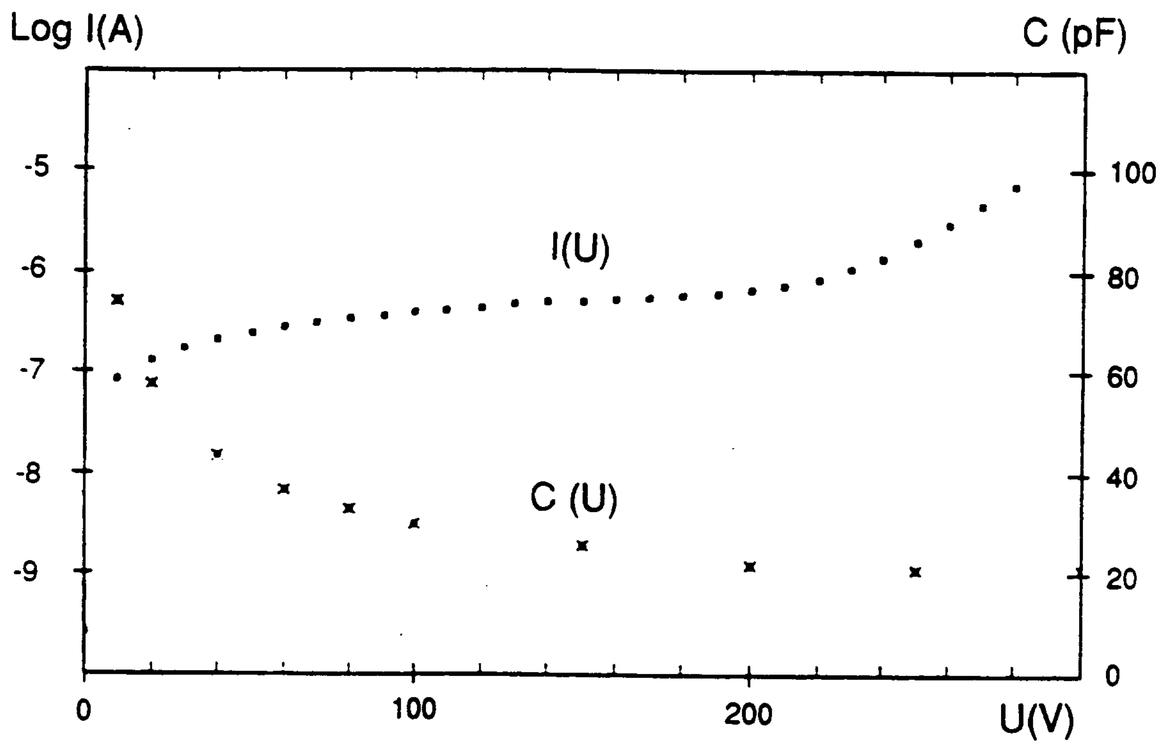


Fig. 18. Typical volt-ampere (VA) and volt-farad (VF) characteristics for one of the diodes. The y-axis shows the log of the current in amps, and the capacitance in pF.

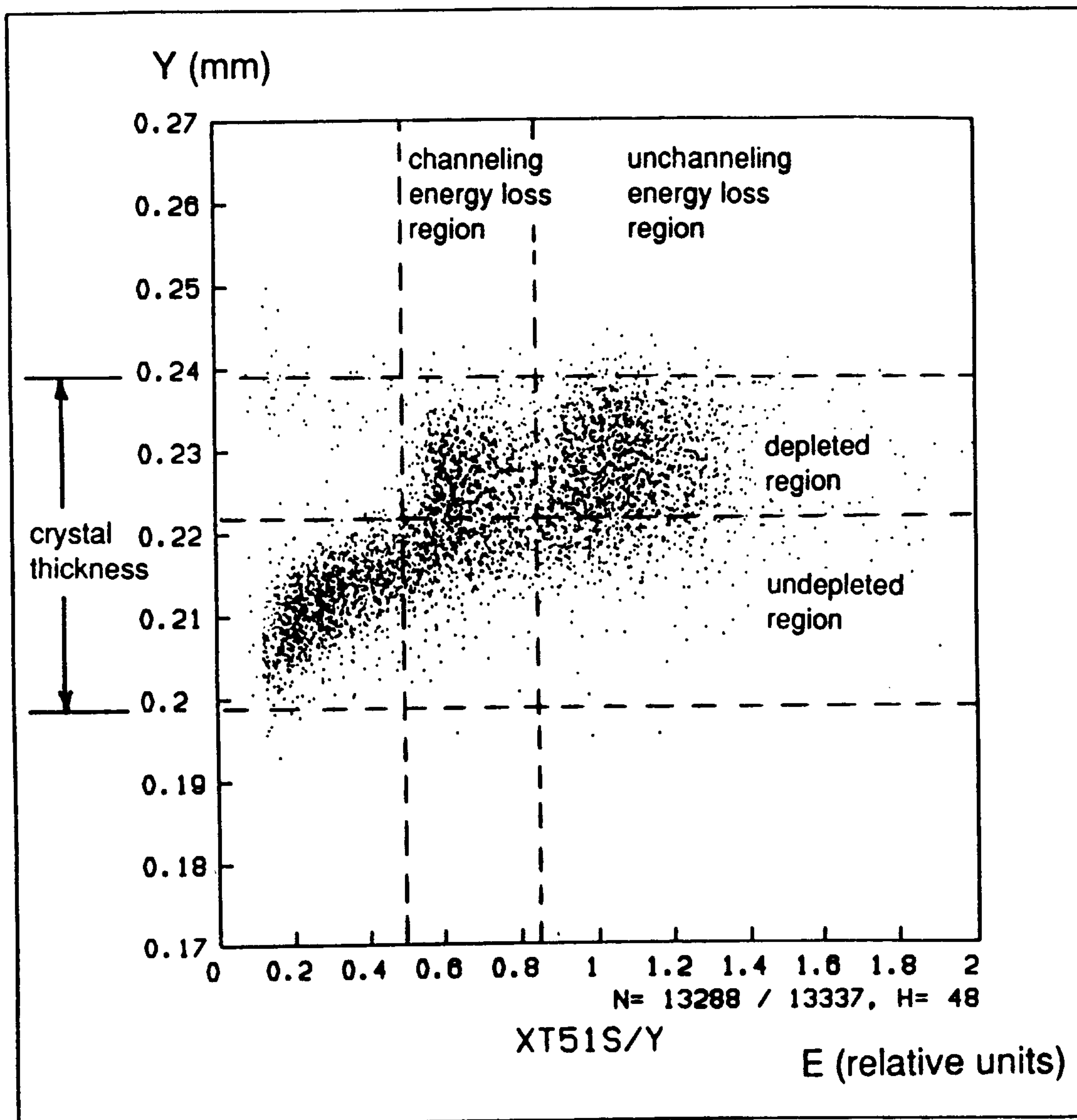


Fig. 19. Distribution of the energy loss signals from one of the E761 detectors for different depths (Y-direction) in the crystal. The energy loss has been normalized to the most probable random energy loss.

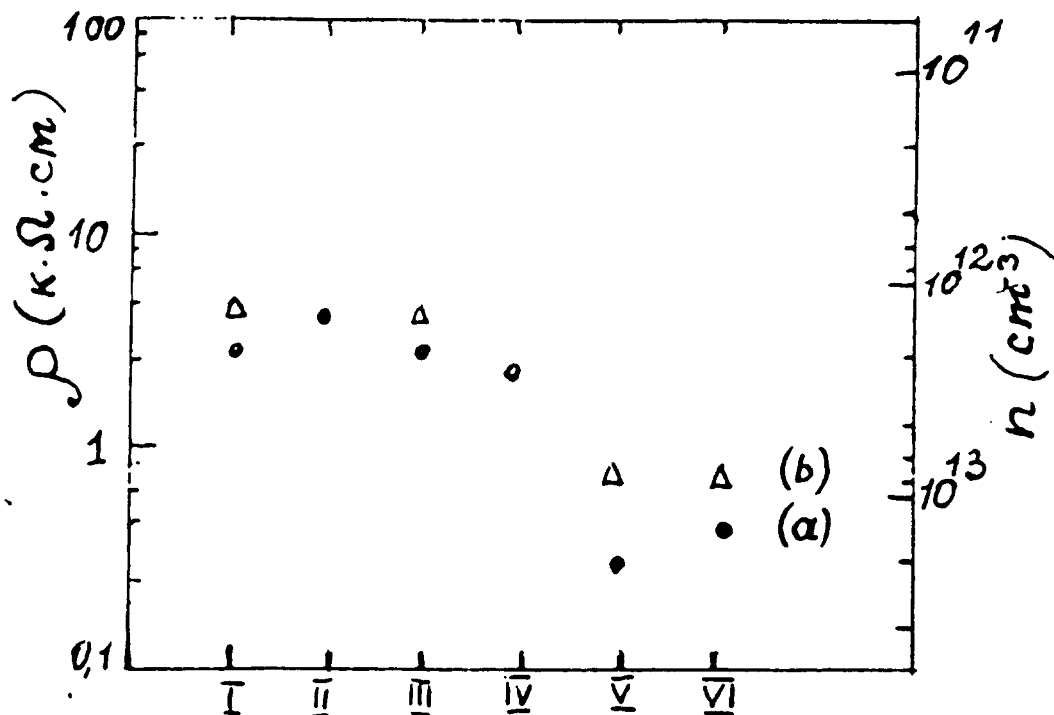


Fig. 20. Variation of resistivity and the associated electron concentration deduced from the resistivity for two wafers (•, ▲) with initial resistivities in the range of 2 and 4 KΩ•cm, after each of the treatment stages I - VI. (Resistivity is in KΩ•cm.)

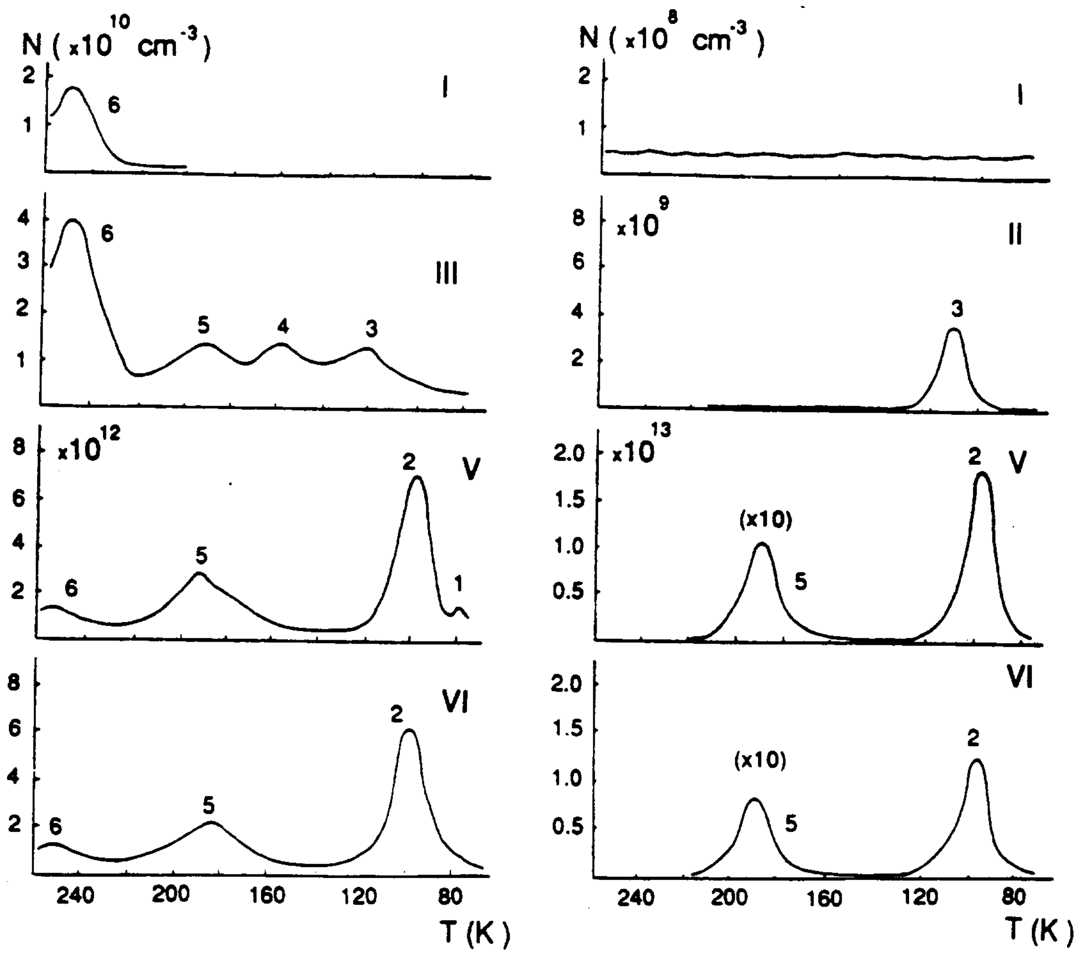


Fig. 21. DLTS measurements for the same samples as Fig. 21 after the high temperature treatments in stages II-VI. Each peak of the spectrum refers to one deep level.

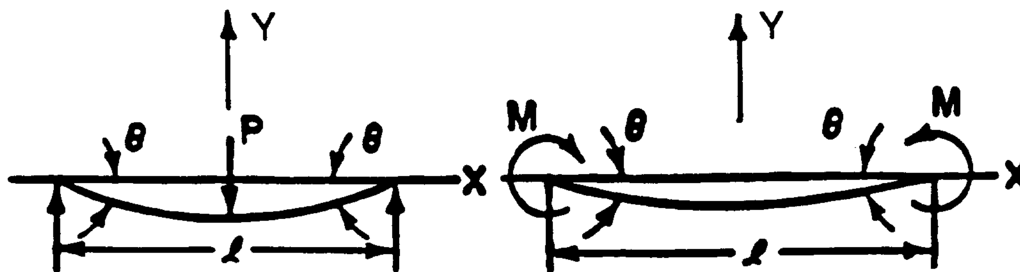


Fig. 22. a) "Concentrated load P at the center" method, the so-called three-point method of bending, b) "couple M at the free ends" or moment method of bending (sometimes called four-point bending).

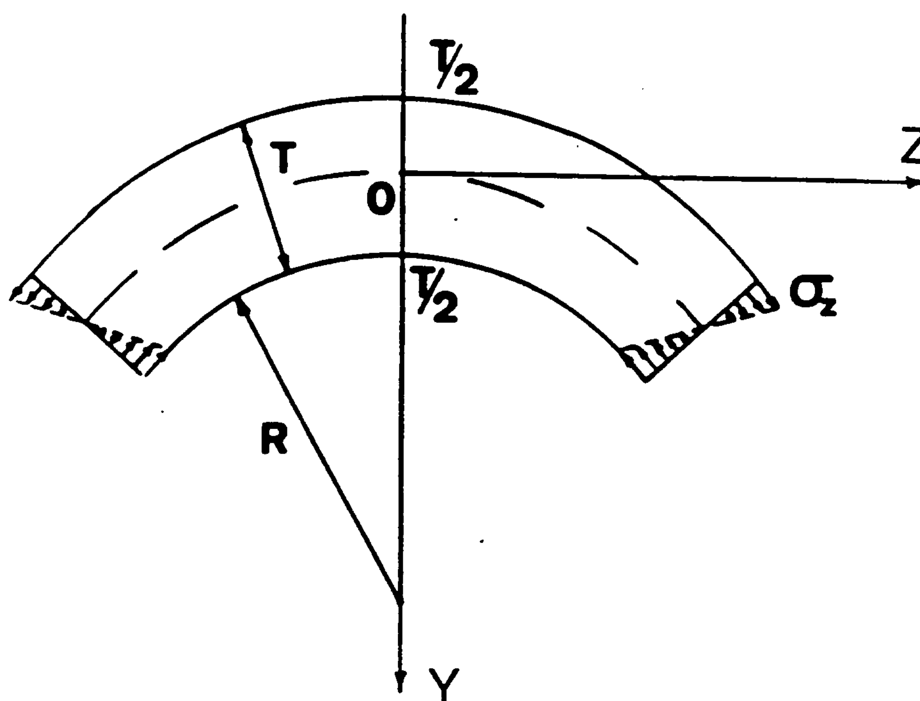


Fig. 23. Schematic illustration showing the distribution of stress over a cylindrically-bent crystal.

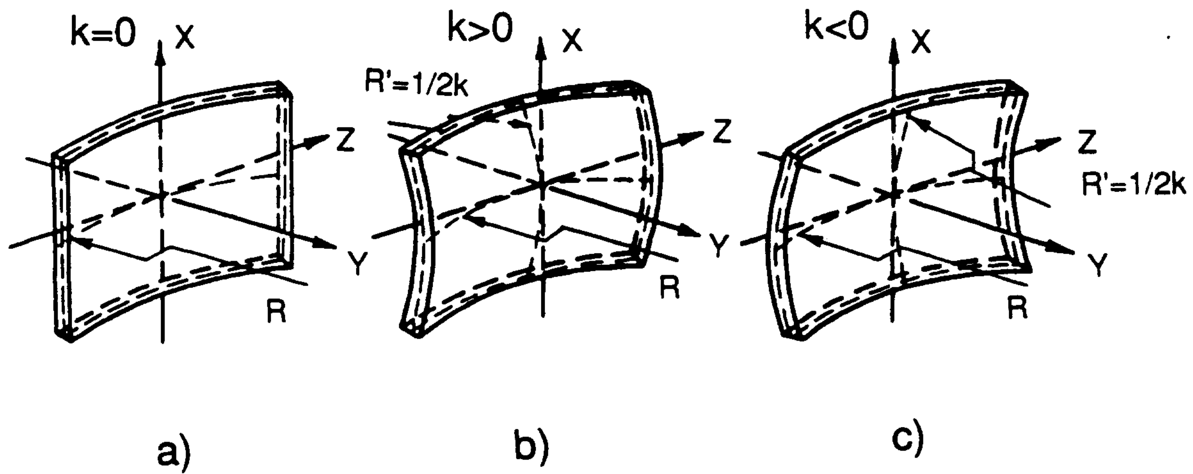


Fig. 24. The equilibrium shape of a plate depends on the topo-logy of the (111) plane, the type of elastic symmetry of the crystal, and other factors. This dependence is related to the sign and value of k (see text).

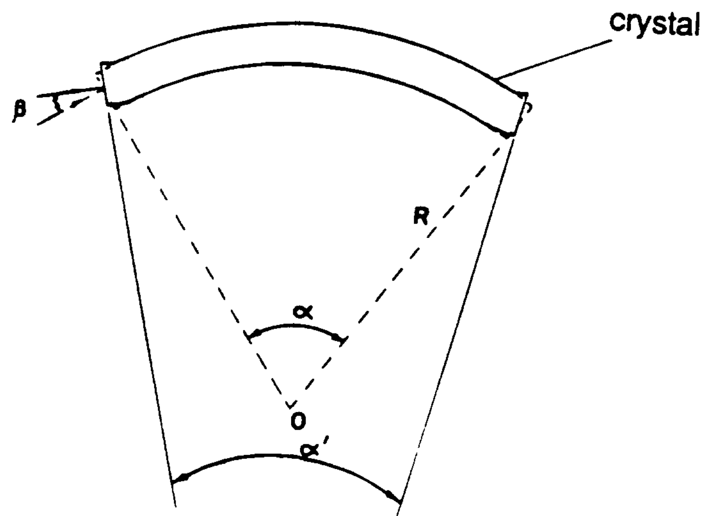


Fig. 25. In the Leningrad experiment the plate bent around a cylinder really had the more complicated shape at its ends shown here.

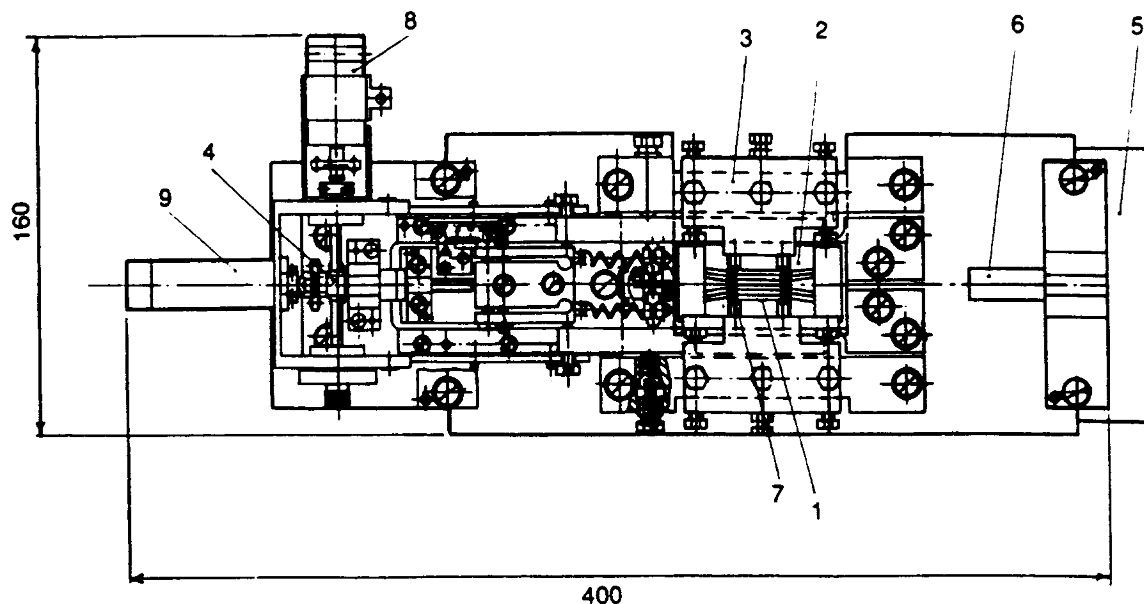


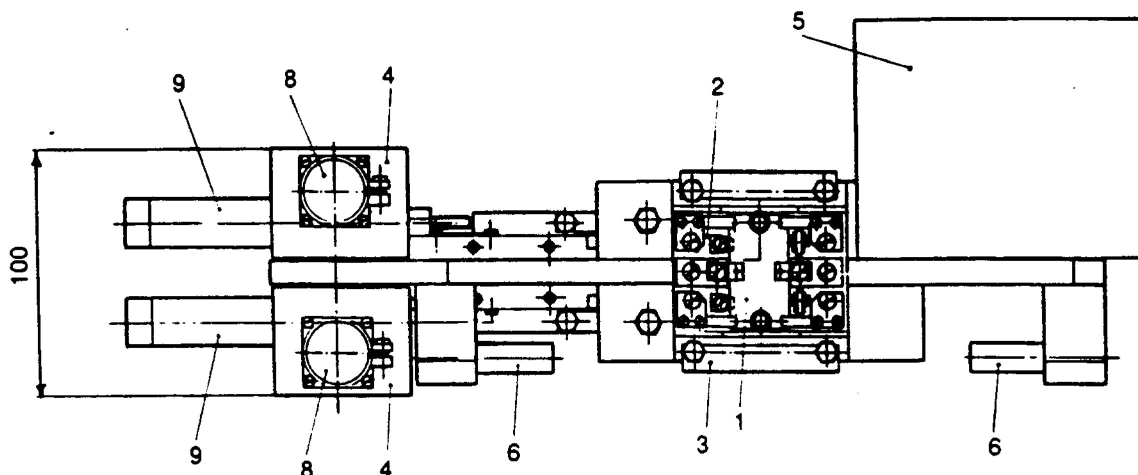


Fig. 26. The E761 device has several principal parts: (1) seven silicon crystals, (2) a crystal support structure, (3) a mechanism for manual rotation relative to other parts of the bending device, (4) two remotely-controlled mechanisms to change the crystal bending angle for the downstream and upstream ends of the crystals, (5) a mount for holding the pre-amplifiers for the semiconductor detectors on the surface of the crystal, and (6) a goniometer that rotates the bending device around a horizontal axis.

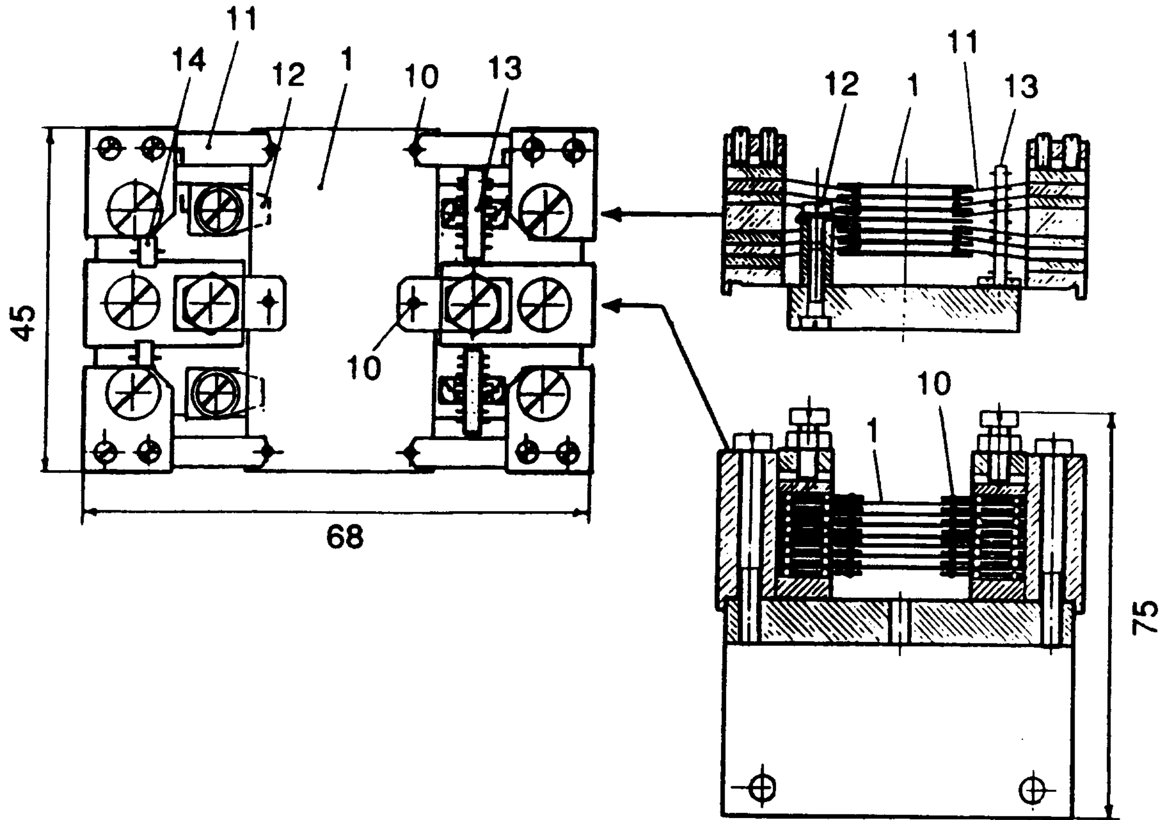


Fig. 27. Plan view of the crystal support structure (2) as well as cross sections of the central and end parts. The three upper and three lower crystals were supported on precision 1.5 mm diameter steel balls at the center part of the long edge of the crystals. The ends of the crystals were separated from each other by small ball-bearings.

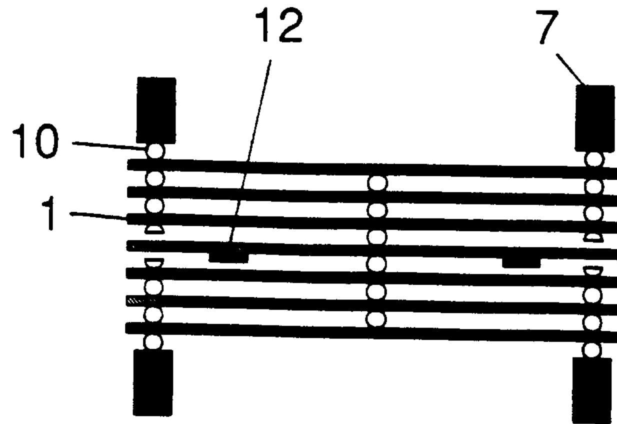


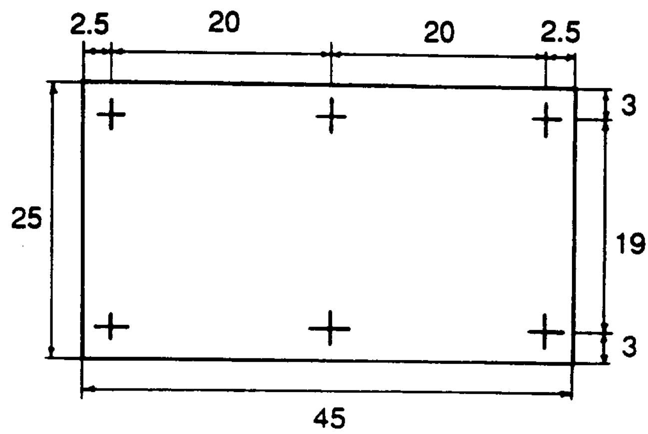


Fig. 28. Schematic illustration of the bending method. It was a typical three-point scheme of bending. The points of contact on the plate are also shown.

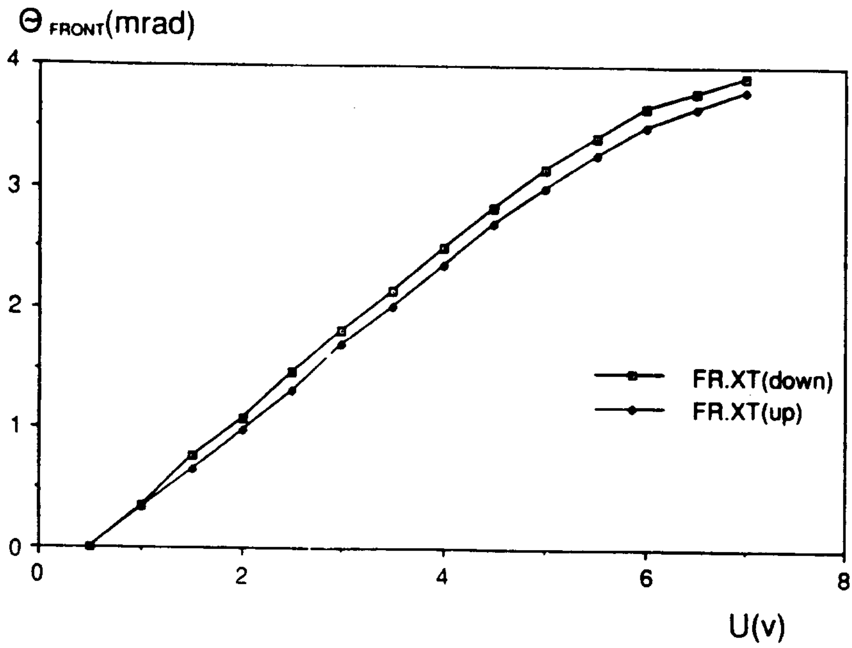


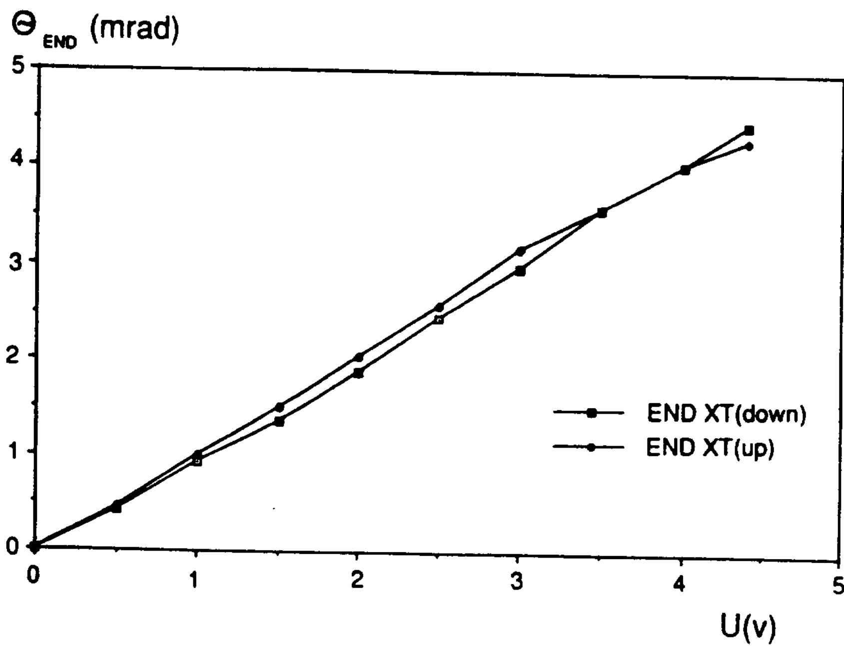


Fig. 29. Relations between potentiometer voltage and the bending angles for upper and lower crystals for a) upstream and b) downstream ends of the crystals.

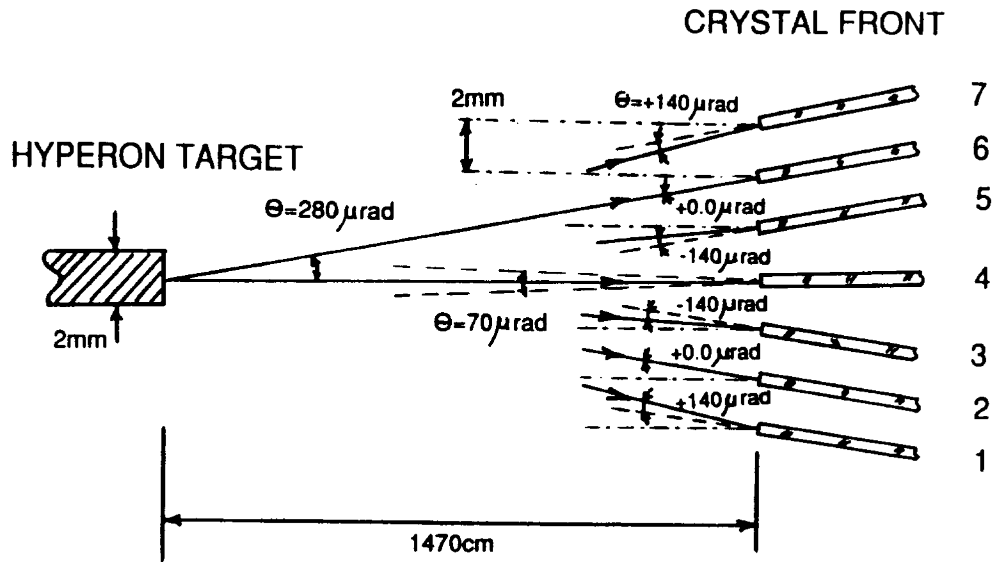


Fig. 30. a) Angular orientation of the crystals was related to the distance from the production target to the upstream edges of the crystals for upstream end.

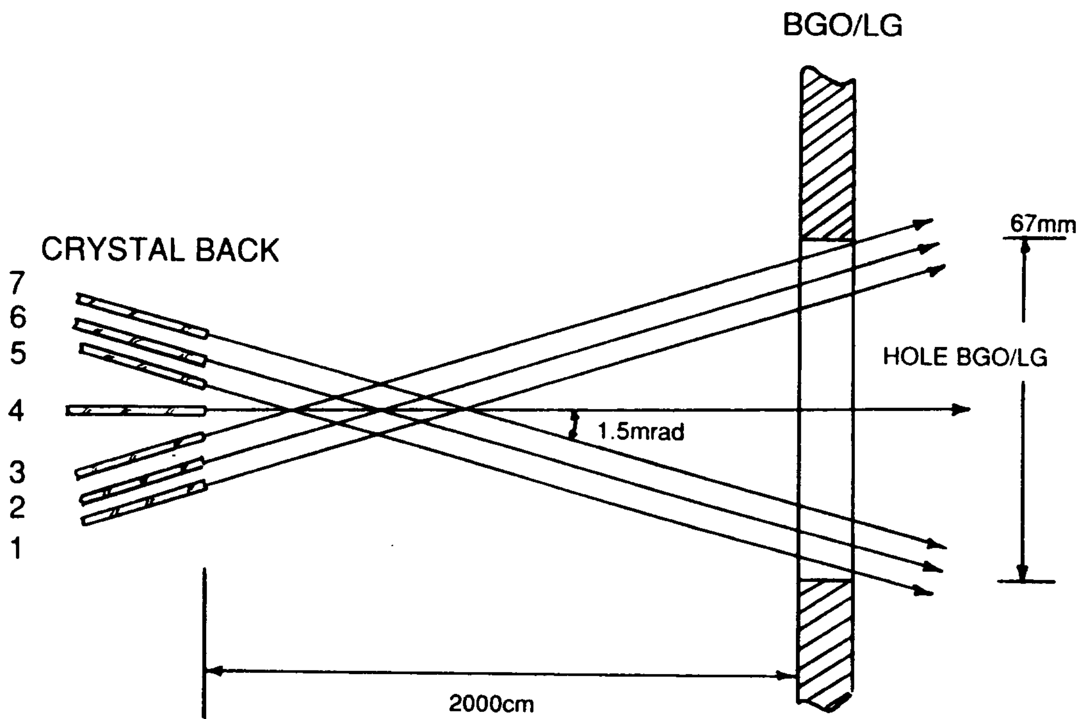


Fig. 30 b) Illustrates the situation for downstream ends of crystals.

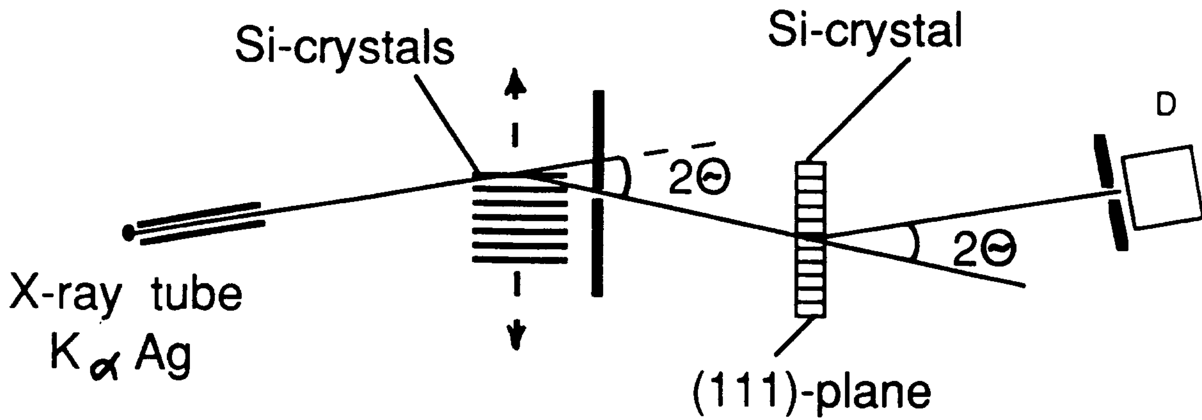


Fig. 31. a) Side view of the two-crystal x-ray diffraction spectrometer geometry used to orient the crystals before the E761 experiment.

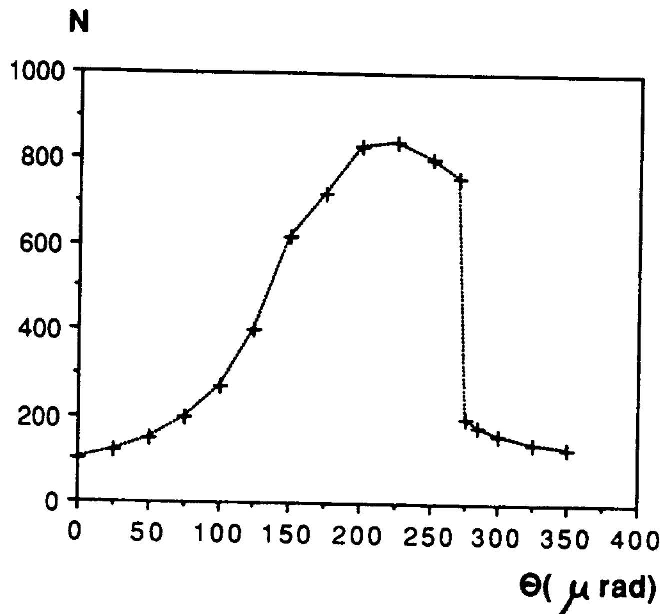


Fig. 31 b) Typical diffraction line from the spectrometer. The sharp edge is determined by the angular position of the plate edge under study. The width of the line results from the curvature of the portion of the bent crystal that was illuminated with x-rays.

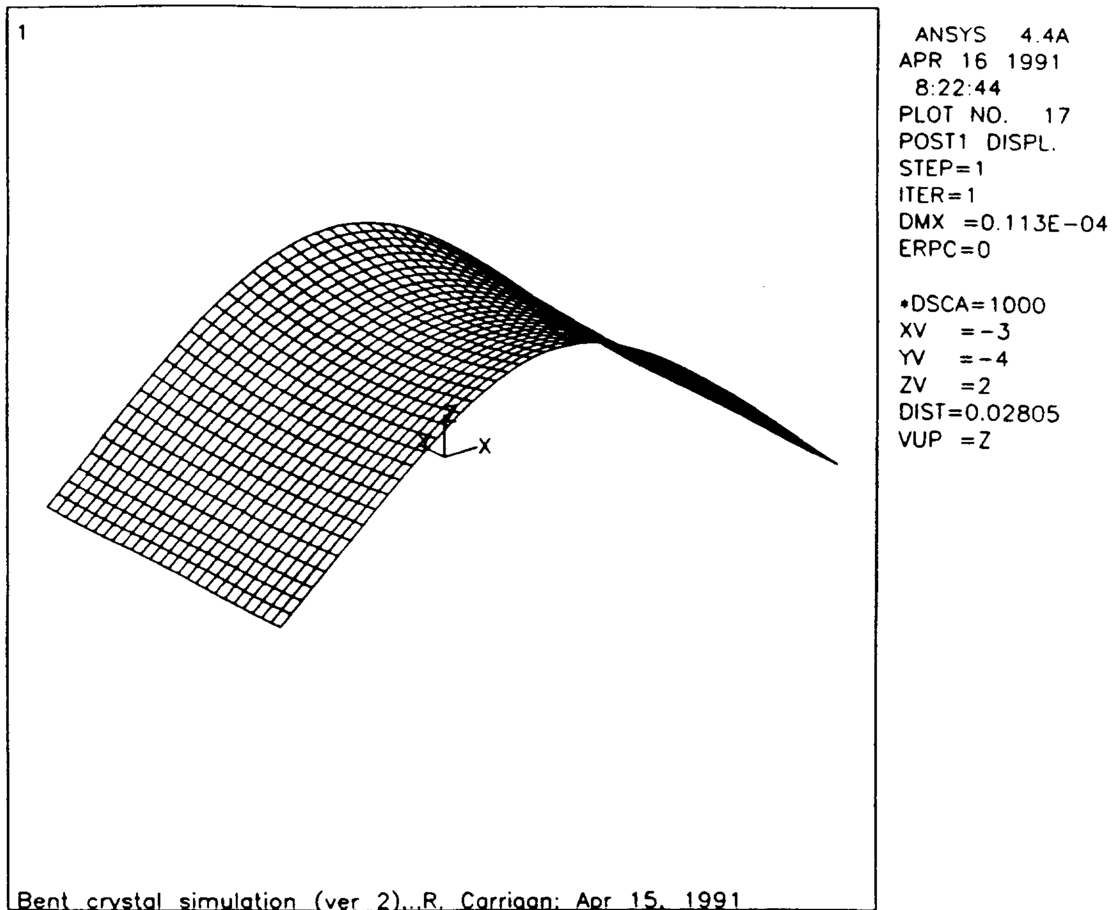


Fig. 32. a) ANSYS simulation showing a three-dimensional view of the crystal for the E761 bend angle of 1.5 mrad. (z on diagram corresponds to hyperon y, x on diagram to hyperon z.)

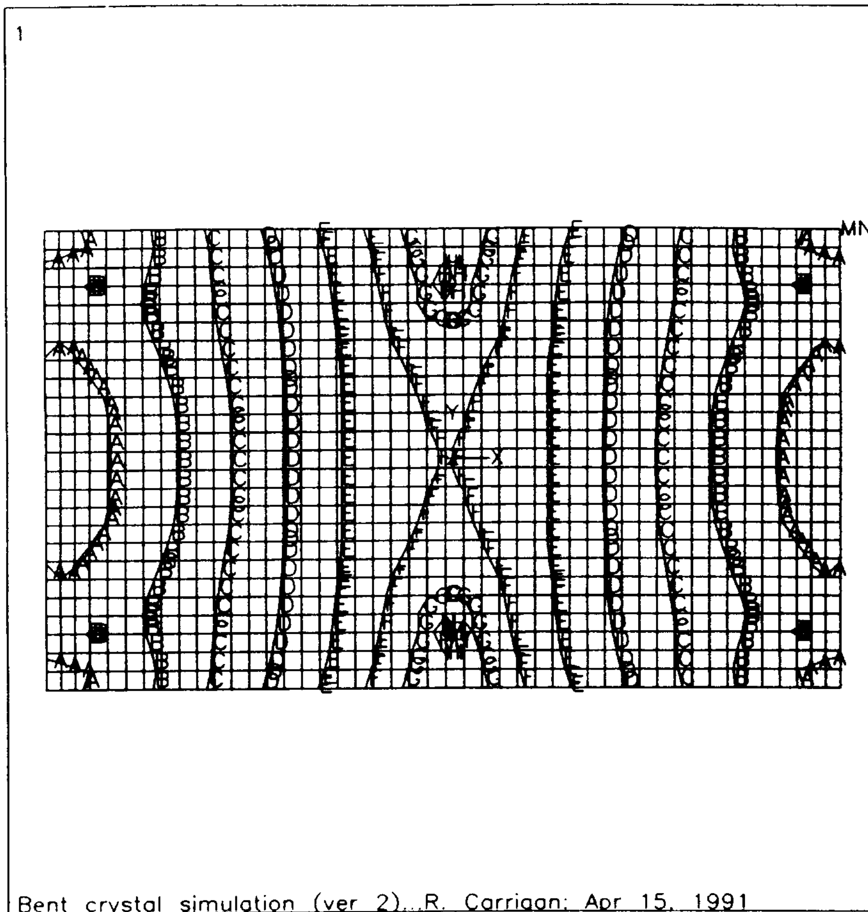


Fig. 32 b) Distribution of stresses in the crystal. Units are in megapascals (MPa).

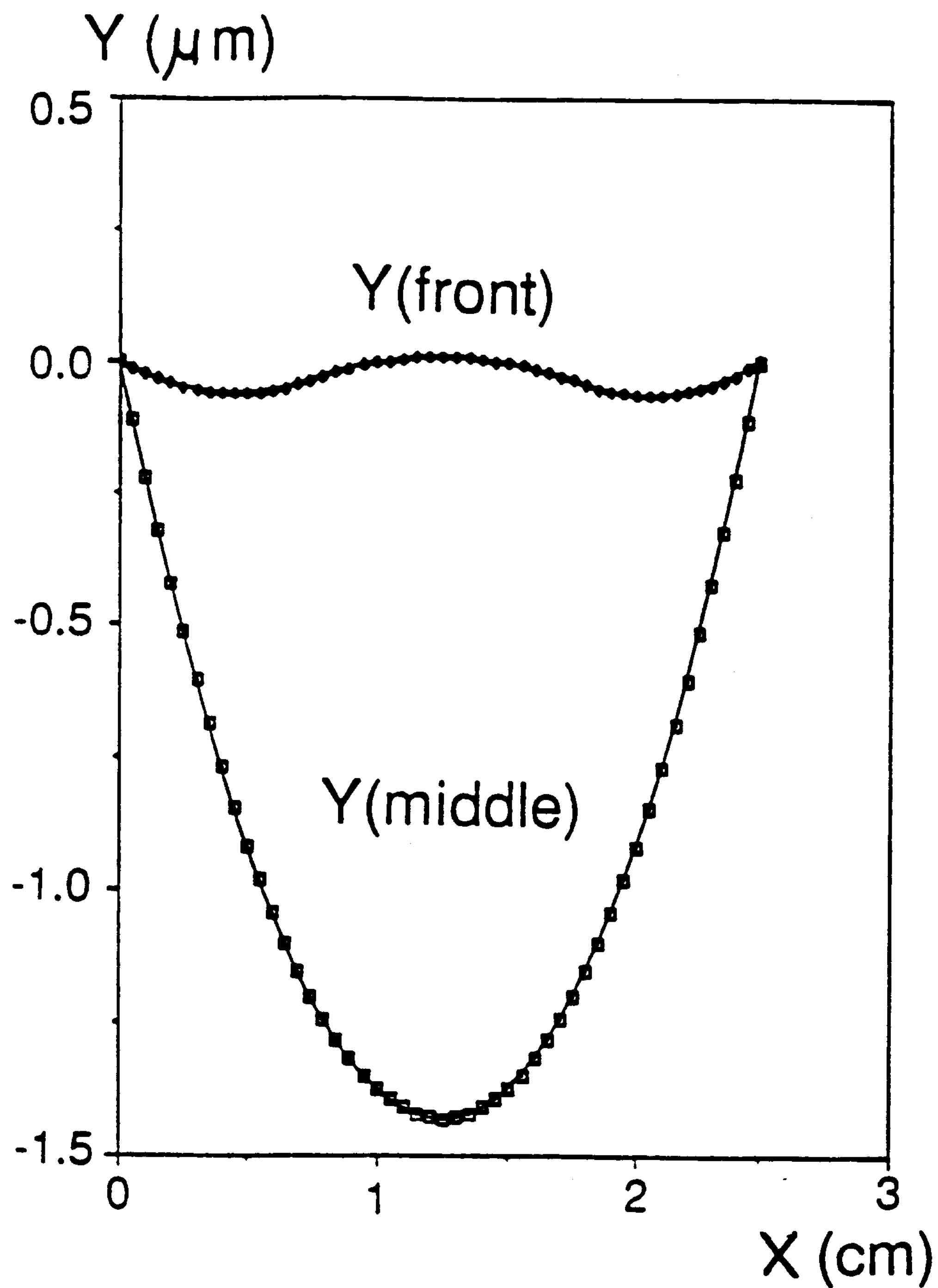


Fig. 33. (XY) cross-sections of the E761 crystal for the upstream end and the mid-section. Y values are in μm. Most of the change of curvature comes from the middle section.

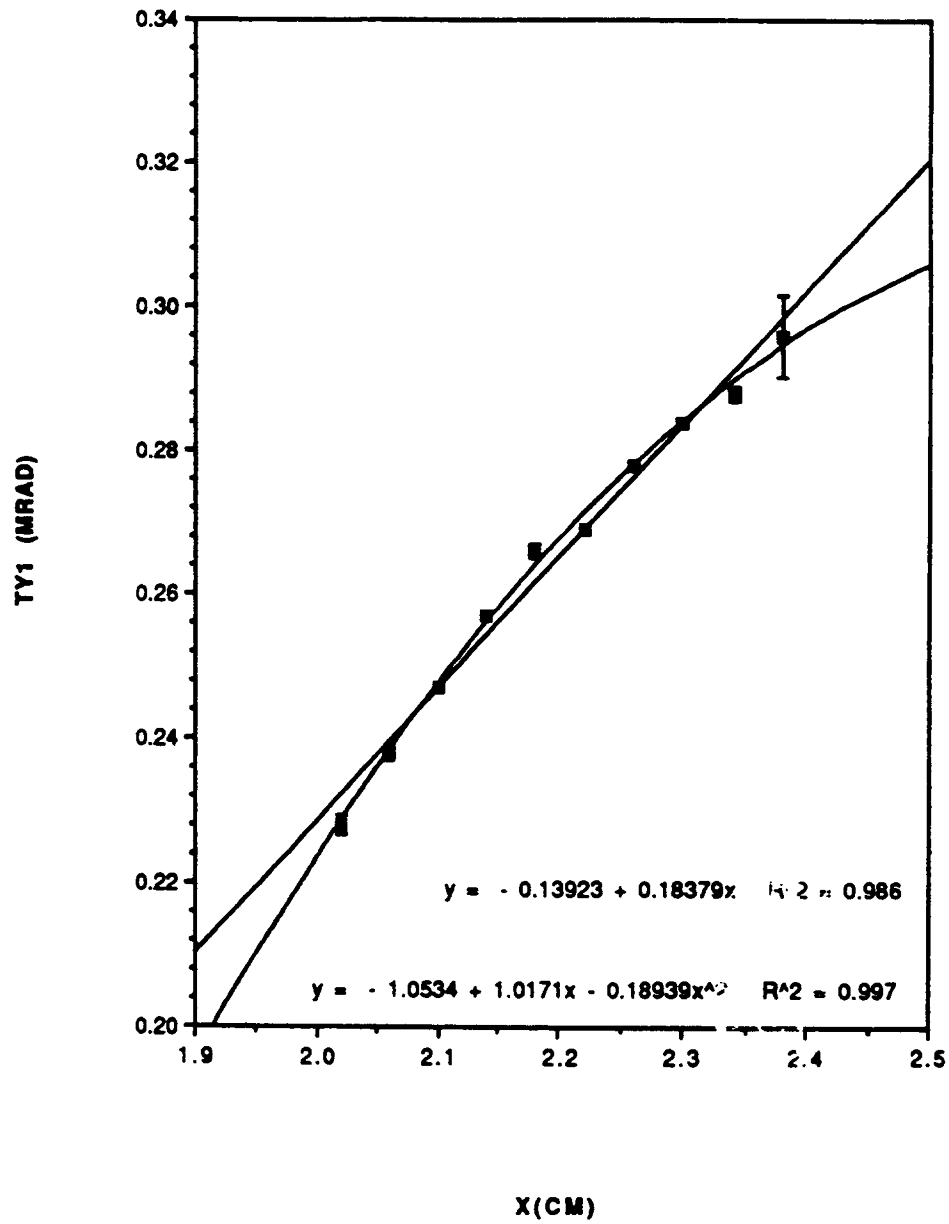


Fig. 34. Entrance angles (TY1) across the crystal for the upper crystal. Linear and quadratic fits to the data. Angles are in mrad.

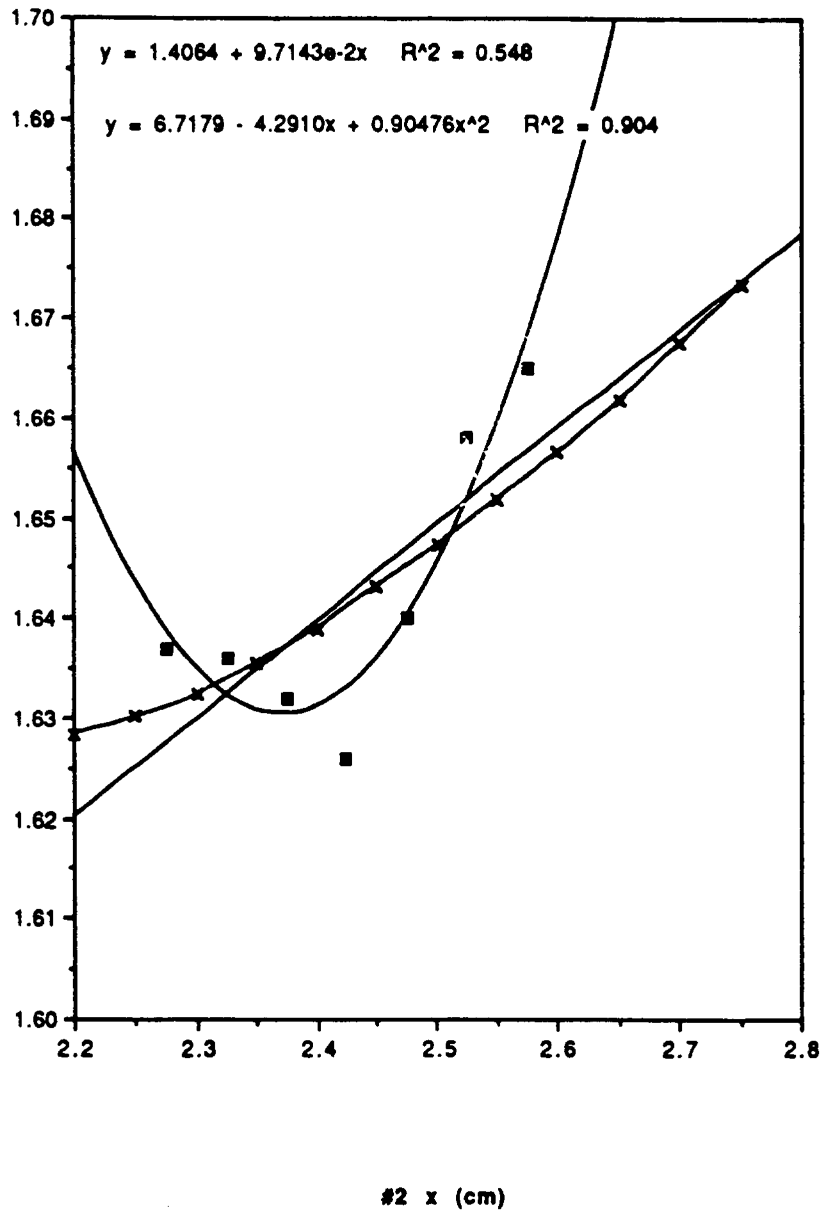


Fig. 35. Variation of DTY (mrad) for the lower crystal including linear and quadratic fits. The ANSYS simulation adjusted to place the minimum curvature at x = 2.05 cm is also shown (with x's).